Q. J. R. Meteorol. Soc. (1999), **125**, pp. 2909–2935

Tropical-wide teleconnection and oscillation. I: Teleconnection indices and type I/type II states

By A. NAVARRA*, M. N. WARD† and K. MIYAKODA
Istituto per lo studio delle Metodologie Geofisiche Ambientali, Italy

(Received 4 August 1997; revised 26 January 1999)

SUMMARY

The tropical oscillation of the ENSO–monsoon (El Niño Southern Oscillation–Asian monsoons) system is studied based on 34-year simulations of an atmospheric general-circulation model with specified sea surface temperature (SST), together with some observed data for the same period. In particular, two indices are studied: the first is the generalized index of Indian monsoon rainfall (IMR), and the other is an index by which the interaction/non-interaction between the ENSO and the Indian monsoon system is assessed.

In order to examine the validity of the first index, the Indian subcontinent and the near-equatorial western Pacific were selected as two key locations. They correspond, approximately, to the dominant regions in the first empirical orthogonal function of precipitation, for boreal summer and winter, respectively. These two regions form the western rim of a 'horseshoe' teleconnection pattern in their respective seasons. The time coefficients of empirical orthogonal function mode 1 in the two seasons are taken as the key indices which are referred to as the Tropical-wide Oscillation Index (TOI).

Having defined the spatial patterns in both seasons, the lead–lag teleconnection structure associated with the ENSO–monsoon system is studied; the result is that the TOI for boreal summer is more useful than the TOI for boreal winter for identifying the lead–lag nature of the ENSO–monsoon. The new index is then related to traditional indices like the IMR and the Southern Oscillation Index, but proves to be a more comprehensive index for lead–lag correlations with key variables, while the latter, the TOI for winter, has no precursory signal for the Indian monsoon for the following summer.

The second index is the Walker circulation Index (WAI), which represents the eastward/westward shift of the updraught region of the Walker circulation. It is proposed that the WAI can usefully distinguish between years when the ENSO–monsoon oscillation operates (type I) and years when it does not (type II). If the SST in the key region has a climatologically close-to-normal condition, the state of the coupled equatorial system is in type II. On the other hand, if the deviation from climatology is large, the tropical-wide oscillation will continue to be active; these years are type I. Elimination of the type II years from the data significantly enhances the time-lagged correlations between the TOI and some key variables, such as SST. As a result, the biennial oscillation becomes clearer.

KEYWORDS: Modelling Observations Statistical analysis

1. INTRODUCTION

Variations of sea surface temperature (SST) in the eastern and central equatorial Pacific have a considerable impact on the global atmospheric circulation and climate. The El Niño Southern Oscillation (ENSO) is the most organized and distinct phenomenon, being concentrated in the tropical Pacific. However, it is traditionally supposed (Walker and Bliss 1932; Troup 1965; Trenberth 1975) that the Pacific process is a part of the whole activity of the Southern Oscillation (SO).

There have been many studies concerning the Indian monsoon and its relation with SST variation in the equatorial Pacific—for example, Shukla and Paolino (1983), Rasmusson and Carpenter (1983), Nicholls (1984), Barnett (1985), Gordon (1986), Yasunari (1985), and Meehl (1987). Based on these preceding works, Yasunari (1991) proposed the idea of the 'monsoon year'. The starting point of the whole cycle is shortly before the summer monsoon, and the Indian summer monsoon rainfall (IMR) is a key variable. Depending upon the strength of the IMR, the subsequent chain of events over the equatorial Pacific takes one of two paths, leading to the component of the tropospheric biennial oscillation (TBO).

* Corresponding author, present address: Center for Ocean–Land–Atmosphere Studies, 4041 Powder Mill Road, Calverton, MD 20705-3106, USA.
† Also affiliated to The University of Oklahoma, USA.

Concurrently, the UK Meteorological Office (UKMO) was investigating Sahel rainfall (SahelR) (Folland *et al.* 1986). They (Ward, personal communication) noticed some evidence that pointed to the existence of two types of ENSO–IMR/SahelR relationships: ENSO affects SahelR/IMR significantly, and ENSO does not affect the monsoons. The demarcation for these two types is likely to be determined by the SST zonal gradient along the equatorial Pacific. In the first situation the effect of ENSO is amplified over a wider area of the tropics, i.e. the Indian and the north African sectors, which is termed the Tropical-wide Oscillation (TO). In contrast, for the second situation the effect remains localized to the tropical Pacific.

2. Background and issues

(*a*) *Monsoon year scenario*

Yasunari (1990) (hereafter referred to as Y90) presented a longitude–time composite anomaly diagram of SST and of the zonal component of wind at 700 hPa along the equator, in which two consecutive IMR years are plotted in the time coordinate. This diagram shows that the ascending locations of the Walker circulation (Bjerknes 1969) vary from west to east, associated with wet/dry IMR, and hence associated with El Niño. A similar diagram can be constructed for the case of La Niña (see Philander (1990)). In other words, Yasunari's scenario starts from a wet or dry IMR and continues to the next year but with opposite sign, when finally the process in the previous monsoon year is effectively forgotten or 'washed out'.

In order to formulate this scenario, we propose two indices to represent the outstanding features in the domain of ENSO and Asian monsoons. One index represents the distribution and intensity of precipitation in the tropical belt, the other specifies the two types of conditions depending whether or not ENSO affects Asian monsoons.

(*b*) *Tropical oscillation indices*

The importance of the IMR of June–July–August (JJA) for Indian agriculture may be indisputable, but the meteorological significance of monsoon indices for tropical circulations has not been well discussed. Shen and Lau (1995) (hereafter referred to as SL95) have shown a relation between the east Asian summer monsoon and ENSO. This monsoon takes place mostly in the subtropical regions of China (i.e. 20°N–35°N).

On the other hand, the SO index (SOI) (Tahiti/Darwin sea-level pressure difference (Troup 1965)) has been used extensively and effectively as a measure of ENSO. A problem is that the SOI does not adequately represent broader scale tropical phenomena (see Webster and Yang (1992)).

The first index we propose is the first empirical orthogonal function (EOF) of precipitation in the tropical belt (40°N–20°S). Different from IMR or SOI, this quantity is more general in terms of representing a broader area, because the precipitation is distributed over a wider region. EOF mode 1 is referred to as the TO index (TOI). However, in practice, the available rainfall data are limited with respect to locations. Therefore, we first test the feasibility of the precipitation index with the model's rainfall.

In order to explain the second index, let us imagine a swing, on which a young lady is sitting, and beside which a boy stands and pulls the swing by a rope. Two types of situations are considered. If the boy pulls the swing strongly away from the equilibrium position, the swing starts to oscillate with a large amplitude. On the other hand, if he does not pull it sufficiently, the swing does not oscillate. These two situations correspond to the two types of modes. Our hypothesis for the ENSO–monsoon pendulum is that there are two states in which the teleconnection is either effective or ineffective. If the Walker

circulation (particularly the updraught region) is in its climatologically normal position, the teleconnection is not tropical-wide but remains localized, whereas, if the Walker circulation is shifted eastward or westward from its normal position, the teleconnection becomes effective.

If this hypothesis is correct, the notion may contribute to the exploration of the biennial variability. The biennial oscillation is one of the characteristic phenomena associated with the SO (see Pazan and Meyers 1982; Rasmusson and Carpenter 1982). As discussed by Meehl (1987) and Goswami (1995), this may not be a fundamental physical mode, if it is quasi-biennial.

3. Observed data and GCM experiments

(*a*) *The observations*

The observed data used in this paper (Parts I and II) are: (i) Norwich's Climate Research Unit (CRU) gridded dataset of precipitation over the globe, including the Indian as well as the Sahel rainfall, for 34 years from 1961 to 1994 (Hulme 1994), (ii) the UKMO Global (interpolated) Sea Ice and SST (GISST) (Parker and Folland 1991; Rayner *et al.* 1996) which includes data for SST and the ice boundary from 1961 to 1994, (iii) the outgoing long-wave radiation (OLR), from the National Oceanic and Atmospheric Administration (NOAA), measured by satellites from 1979 to 1994, (iv) the blended data of precipitation, based on rain-gauge measurements, satellite sensing, and model results from 1979 to 1994 (Xie and Arkin 1996), and (v) the European Centre for Medium-Range Weather Forecasts (ECMWF) data-assimilation re-analyses (ERA) (Gibson *et al.* 1994) for 9 years from 1981 to 1989. In addition, many of the results were also checked using Oort's (1994) updated analysis of the atmospheric circulation from 1964 to 1994.

(*b*) *The GCM experiments*

The atmospheric general-circulation model (GCM) employed is ECHAM4 with triangular truncation at wave number 30 and with 19 vertical levels. The ECHAM4 model (Roeckner *et al.* 1996) is a fourth generation climate GCM, which has evolved from the medium-range forecasting model at the ECMWF, but significantly modified at the Max-Planck Institute. Aspects of ECHAM3 are summarized by Bengtsson *et al.* (1996), and this model was used in the Atmospheric Model Intercomparison Project (Sperber and Palmer 1996). ECHAM4 has additional changes in the cumulus parametrization and radiation, the former being the so-called 'buoyancy closure' type. Experiments were run with this model from 1961 to 1994, because Oort's data are available for almost the same period. The lower-boundary conditions of the SST and ice boundary are given by the data of the GISST.

A GCM has particular advantages for this type of study, because it can produce many realizations, while the observation is only one realization. In this paper, three solutions will be generated by the model, starting from three slightly different initial conditions. The major reason for the three solutions is to obtain statistically valid results, though more than three is preferable, even in the tropics.

(*c*) *Time series of Indian monsoon indices*

It may be useful to know the model's capability of simulating the tropical precipitation. Extensive investigations have been conducted on the simulation of tropical precipitation with these results (Moron *et al.* 1998). The precipitation was compared with

the observations. Agreement between the model and the observations is fairly good over the Pacific sector (0.85 anomaly correlation for January–February–March (JFM), worse over the Indian sector (correlation 0.22 for JJA, and poor over the Sahel (correlation 0.17 for JJA). The south-east Asian monsoon is overall well simulated, but the ENSO correlation to this monsoon is weaker in the simulations than in the observations. This may be partly related to an overall negative bias in the simulated rainfall over the Indian sub-continent, with too much rain occurring over the ocean.

4. Tropical-wide teleconnection

(*a*) *Teleconnection and its key regions*

Concerning the ENSO, it has been known that the time-scale of the phenomenon is determined by the air–sea coupled process. Yet the atmospheric motions alone can play an important role in remote teleconnection. Indeed, for the ENSO–monsoon phenomenon, the teleconnection process operates, for a large part, through the atmosphere, particularly through vertical velocity (omega) and, accordingly, precipitation. The tropical circulation was discussed in terms of velocity potential by Krishnamurti (1971), and in terms of omega by Lau and Li (1984). They demonstrated that, in boreal summer, the time-mean centres of updraughts are located over India and the Himalayas, and the downdraughts are scattered over the south-equatorial longitudes, and therefore 'a local divergent circulation (regional Hadley circulation)' prevails between the Himalayas and the equatorial Indian Ocean, while the Walker circulation (Bjerknes 1969) is dominant over the equatorial Pacific. In boreal winter, on the other hand, the centres of updraughts are located north of Australia and the downdraughts are scattered in both hemispheres, particularly over the Himalayas.

Our interest in this paper is year-to-year anomalies from the mean climatological pictures of vertical motion, and, therefore, precipitation which are described in the above papers. Wallace and Gutzler (1981) introduced the global teleconnection map, connecting centres of high correlation of geopotential-height anomalies between two locations on the globe. In a similar way, one could calculate correlations of omega for the tropics. However, what is needed in the present study is not only the simultaneous, but also the time-lagged, teleconnectivity; the time range of our interest covers plus and minus 2 years, at least. A way of handling such a problem would be to set up a three-dimensional teleconnectivity map with two spatial dimensions and one temporal dimension. We consider two approaches. The first one is to calculate the instantaneous (zero-lag) correlations between a host index (such as TOI) and a target variable at all locations (such as omega); and then produce further maps introducing lags between the host and target variables. The second approach is to construct longitude versus time-lag diagrams of correlation, as SL95 did.

In order to find the reference region, an EOF analysis is applied to the 34-year series of the model's precipitation. Figure 1 is an example for two particular seasons, i.e. for July–August–September (JAS) and JFM. It is a salient feature that maximum values are located over the Indian continent and the equatorial Indian Ocean in JAS (Fig. 1(a); explains 32% of variance); they traverse to the south-east in the northern autumn (not shown); then move to the western near-equatorial Pacific in JFM (Fig. 1(b); explains 42%); and finally come to the western edge of the South Pacific Convergence Zone (SPCZ) in April–May–June (AMJ), though the percentage of mode 1 in AMJ (not shown) is only 22%. In short, the maximum position of EOF 1 migrates with season from India through the western Pacific. The path of seasonal migration reminds one of the figure shown by Meehl (1987), though his variables are not only precipitation,

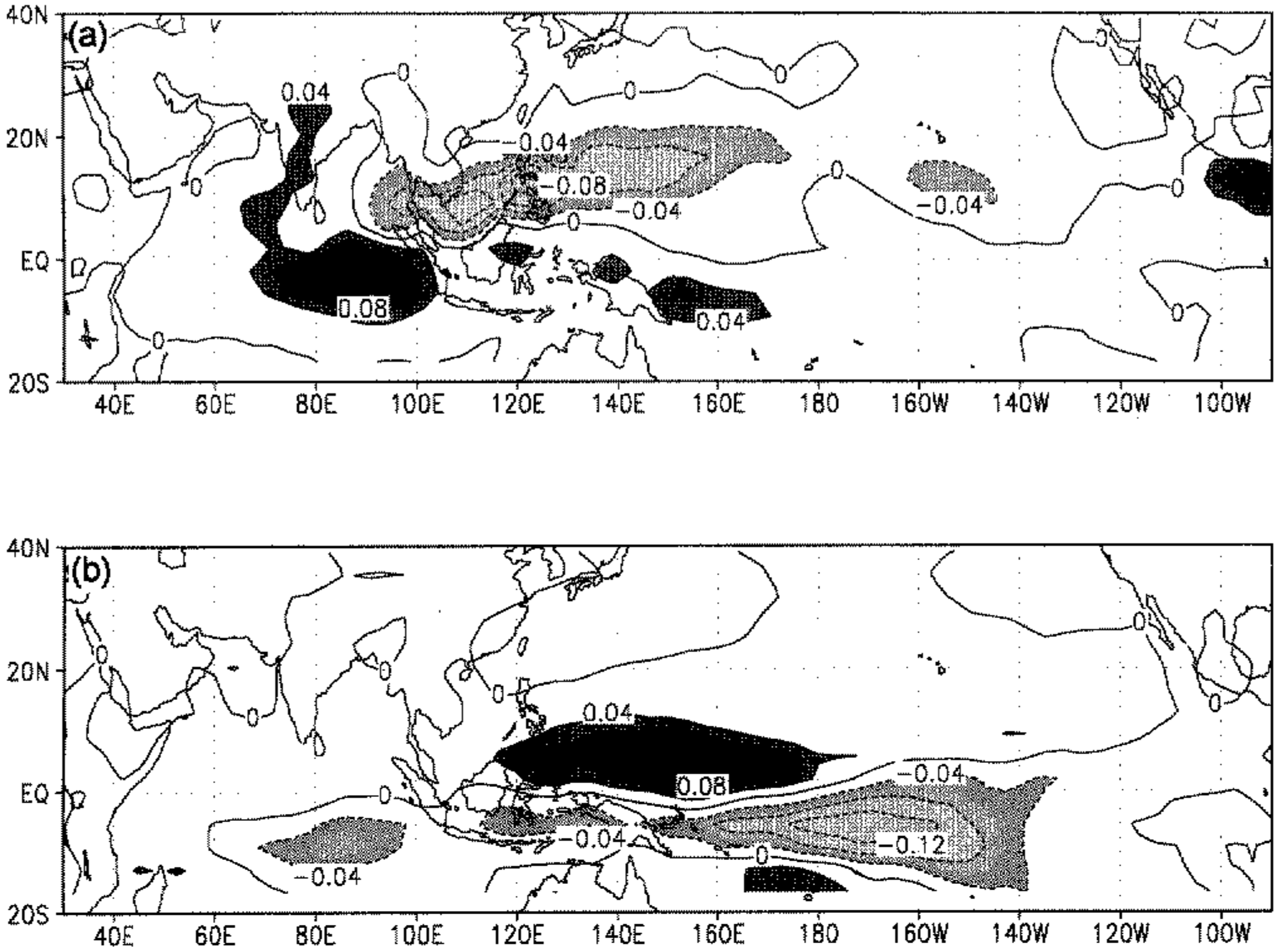

Figure 1. Empirical orthogonal function mode 1 (EOF 1) distribution of the normalized anomalies of precipitation for (a) July–September and (b) January–March. The domain is the tropical belt between 40°N and 20°S. Three EOF 1s of three model runs are averaged. Areas greater than 0.04 are dark shaded, and less than −0.04 are light shaded.

but also sea-level pressure and OLR, and besides they are monthly mean climatologies instead of anomalies. We take two of the most outstanding maxima of anomalies along this path, i.e. the regions A and Z (Fig. 4) as key sites for JAS and JFM respectively. The Z-region is located east of the Philippine Islands, which is slightly east of Meehl's climatological maximum for JFM.

(*b*) *Significance of the precipitation in the regions A and Z*

Taking the TOI(JAS) as the host variable, correlations are calculated between the TOI and precipitation of the whole domain; first, for JAS each of three model realizations of precipitation is used, and then correlations are averaged (Fig. 2). The robustness of the EOF patterns is confirmed because the EOF 1 for JAS (Fig. 1(b)) resembles well the correlation map of precipitation referred to TOI(JAS) (Fig. 2(b)), and similarly EOF 1 for JFM (Fig. 1(b)) resembles the correlation map of precipitation referred to the region Z (130°–150°E, 15°–5°N) (Fig. 2(b)).

As expected, the area of highest correlation with the TOI(JAS) corresponds approximately to the area of the IMR(JAS); this is region A, and that of the TOI(JFM) corresponds to region Z. The geographic maps of these teleconnections are characteristic of the 'horseshoe' patterns with the reference regions, A or Z, at or near their western ends.

So far, the good consistency among several representations has been described. Figures 1 and 2 are model results, and they are consistent. The same types of maps were produced by using the model's omega at the 500 hPa level. They are very similar to Figs. 1 and 2. In order to check the validity of these model results, the Xie–Arkin

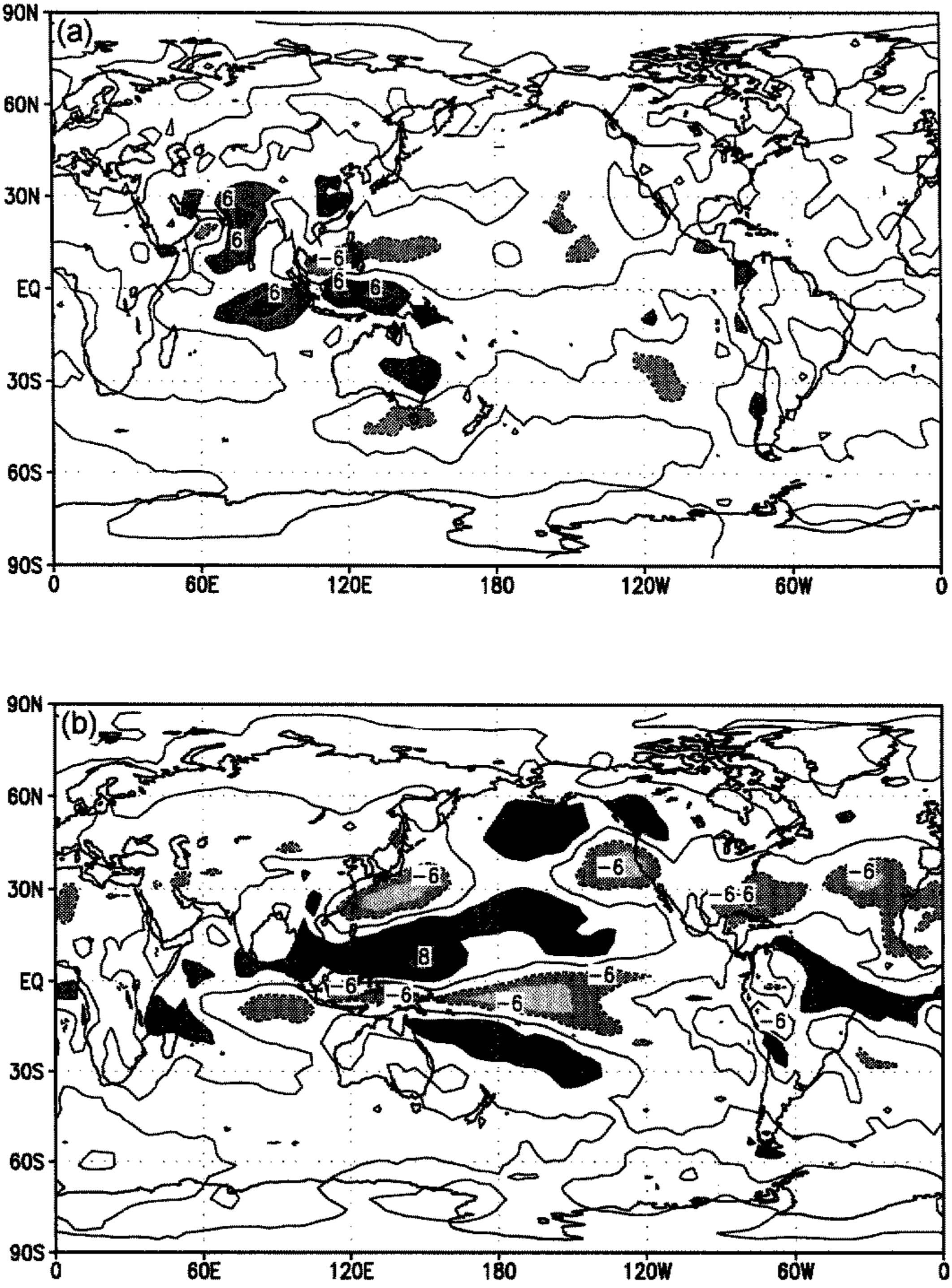

Figure 2. Correlation (×10) between the Tropical-wide Oscillation Index (TOI) and the model's precipitation. The host variable is (a) the model's TOI for July–September (JAS), and (b) the model's TOI for January–March (JFM).

data are used as the proxy observed rainfall (Fig. 3). Inspection of Figs. 2 and 3 reveals: (1) The most pronounced rain configurations for both seasons are the horseshoe patterns with the central axis at the equator. The horseshoe is surrounded by the outer rims in the western periphery. The southern branch of the rim corresponds to the SPCZ, and there is the counterpart for the northern hemisphere (tentatively referred to as the Northern Pacific Convergence Zone (NPCZ)). (2) The results in Fig. 3 are overall in agreement with the previous figures. Particularly, Fig. 3(b) supports the consistency in the JFM case. However, the comparison of model and observed maps for JAS reveals a serious difference. The model fails to produce the teleconnection with the NPCZ in JAS (or perhaps misplaces it over central China); and the central axis along the equator is shifted northward in the model. (3) In the Xie–Arkin data, the correlation values do not decrease so fast with distance from the centres of action. In particular, in JAS the Xie–Arkin data suggest that positive correlations extend westward to India and, also, into the tropical Atlantic, the Caribbean and, more weakly, into the Sahel of Africa. The model does not capture the extension.

The above investigation suggests a central role for teleconnectivity from region A in boreal summer and region Z in boreal winter (see Fig. 4). In this respect, the correlation maps (Figs. 2–3) reveal that the major influence domain of the TOI(JAS) or IMR(JAS) tends to be confined meridionally to the tropics, and longitudinally from the dateline westward to 60°E (and maybe beyond), while the influence domain of the TOI(JFM) spreads poleward of the tropics, as well as eastward longitudinally. The westward extension (or lack of eastward extension) of the TOI(JAS) may be due to the Himalaya mountain barrier and the longitudinal position of the heat source (region A). This argument has been supported by a theoretical study, using an anomaly model (Navarra, personal communication); see also Rodwell and Hoskins (1996).

(*c*) *Lag correlations with the region A*

We now examine the lead and lag teleconnection structure, using the model's precipitation during JAS as the host index and the model's omega at 500 hPa level as the target variable. In particular, we will consider whether using another season's index (e.g. JFM) as host might reveal additional information on the ENSO–monsoon system. Lag correlations are calculated between the precipitation in the host region, A, and omega in the surrounding areas, i.e. 'target regions', selected from three latitudinal belts, 10°S–10°N, 10°–25°N and 35°–45°N (see Fig. 4), hereafter referred to as the latitudinal belts, B, C and D, respectively, each belt being divided by five longitudinal sections, i.e. 0, 1, 2, 3 and 4, with the longitudinal width of 30°.

As the first step, lag-correlation diagrams for omega as the target are exhibited in Fig. 5, in which curves of all 15 subdomains are shown together. Each subdomain consists of lag and lead correlations on the right- and left-hand sides around the centre line, where 'lag' means that the value in the target region lags in time behind that of the host region, A.

First, using the first GCM run, an analysis for July in the host region (the IMR) is calculated, with target regions leading and lagging by up to 12 months. The analysis is repeated for August and September, and the three sets of results are averaged. The analysis is repeated for each of the three GCM runs, and all results averaged. This procedure was devised to give a good estimate of the monthly lead–lag relations that are occurring around and during the JAS season.

Box 2-C is co-located with India, and hence the zero-lag correlation is very high. Except for this box, correlations are not high (less than 0.5). Some of the pronounced features in Fig. 5 are: (1) Boxes 2-B and 3-B have positive zero-lag correlations.

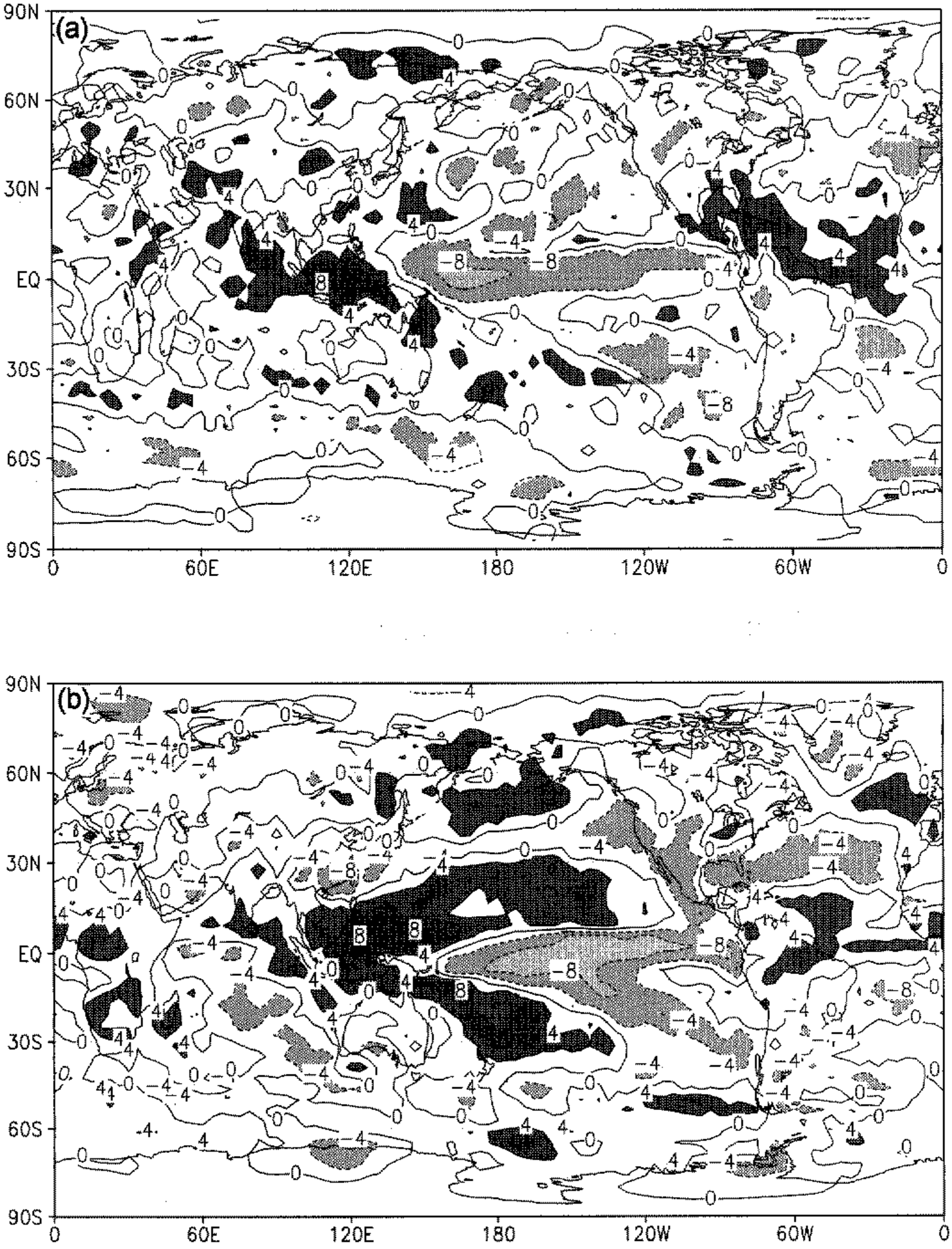

Figure 3. The same as Fig. 2, but the host is the observed TOI(JAS), and the target variables are the observed rates of precipitation, based on the Xie–Arkin data.

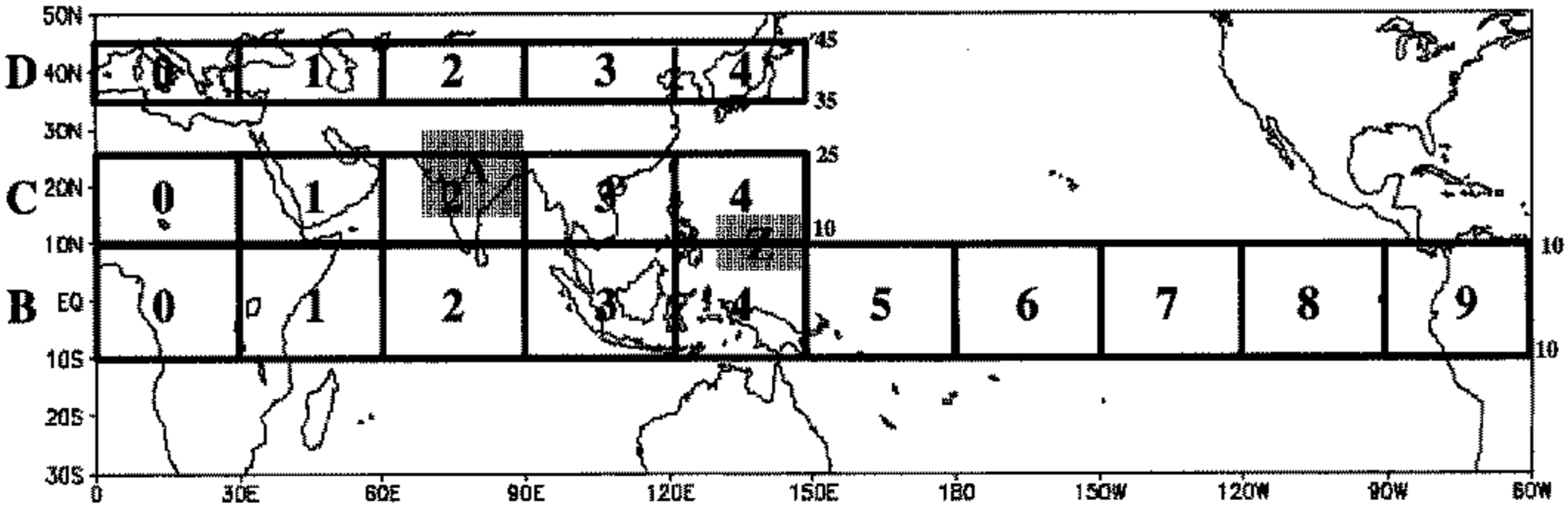

Figure 4. Subdomains used for the diagram in Fig. 5. The extra equatorial subdomains, i.e. boxes 5–9 are used for the diagram in Fig. 6. The key regions A and Z are defined in section 4.

(2) Box 0-C (Sahel) has negative correlations, especially when the Sahel is lagging India, indicating that IMR and Sahel vertical velocity have some interaction in the model. (3) Box 4-C overlaps with the Z-region, and it has negative correlation. (4) Boxes 0-D and 1-D have negative correlations, suggesting that subsidence over the Mediterranean Sea (0 ~ 1 month lag) is associated with monsoon updraughts over the Indian region (see Rodwell and Hoskins (1996)). (5) Box 2-D, north of India, has small negative correlations, indicating that the Kazakhstan area forms a north–south dipole with India (Yanai and Li 1994). (6) Box 3-D corresponds to eastern China (SL95), showing simultaneous positive correlation.

(*d*) *Equatorial teleconnection*

In order to pursue further the teleconnection characteristics, correlation target boxes are confined to the equator (the B-box belt), but extended eastward to the central and eastern Pacific, because teleconnection signals can be easily transmitted along the equator, particularly eastward (Bhalme and Jadhav 1984). Additional boxes are set up: 5, 6, 7, 8 and 9 (Fig. 4).

Figure 6 is the result of this experiment; small circles in the upper row correspond exactly to the same circles in Fig. 5 (IMR(JAS) versus omega). Different from Fig. 5, not only omega but also SST is adopted as a lagged target variable, as Verma (1994) did. Also, the lead and lag periods are extended from 12 to 24 months. Correlation magnitudes are appreciably larger than in Fig. 5, particularly IMR–SST correlations. The small circles in Fig. 6 will be discussed here, while the other lines will be discussed in section 7. The circles reveal the following:

(1) omega-correlation curves and the SST-correlation curves appear grossly similar to each other over the Pacific (boxes 5–9), but not over the Indian sector (box 2).

(2) Boxes 6, 7, and 8 have large negative values with their peaks around 0 month lag. It is of particular interest that these boxes show small positive correlations in the negative coordinate, meaning that there is a lead relationship (6–12 months) from the Pacific to the IMR(JAS), i.e. precursory signals in the Pacific SST for the Indian monsoon.

5. Time–longitude section of correlation with the TOI

(*a*) *Utility of the TOI(JAS)*

Lag-correlation diagrams shown in the previous section are useful for comparing different variables or different latitudes simultaneously, but they are not so convenient

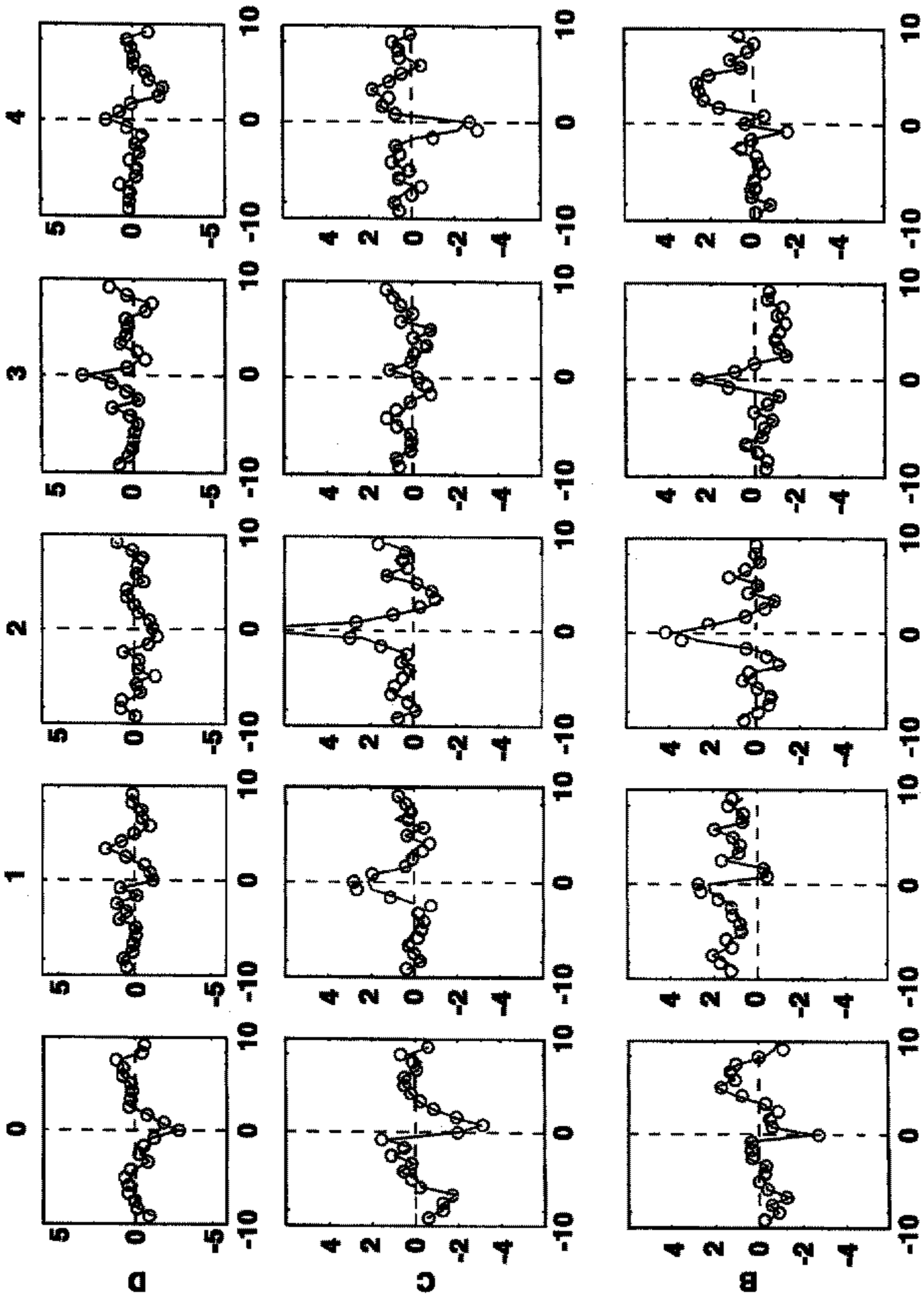

Figure 5. Lag correlations (×10) of model Indian monsoon rainfall for July–September and vertical velocity for the 15 boxes shown in Fig. 4. *x*-axis is lag in months.

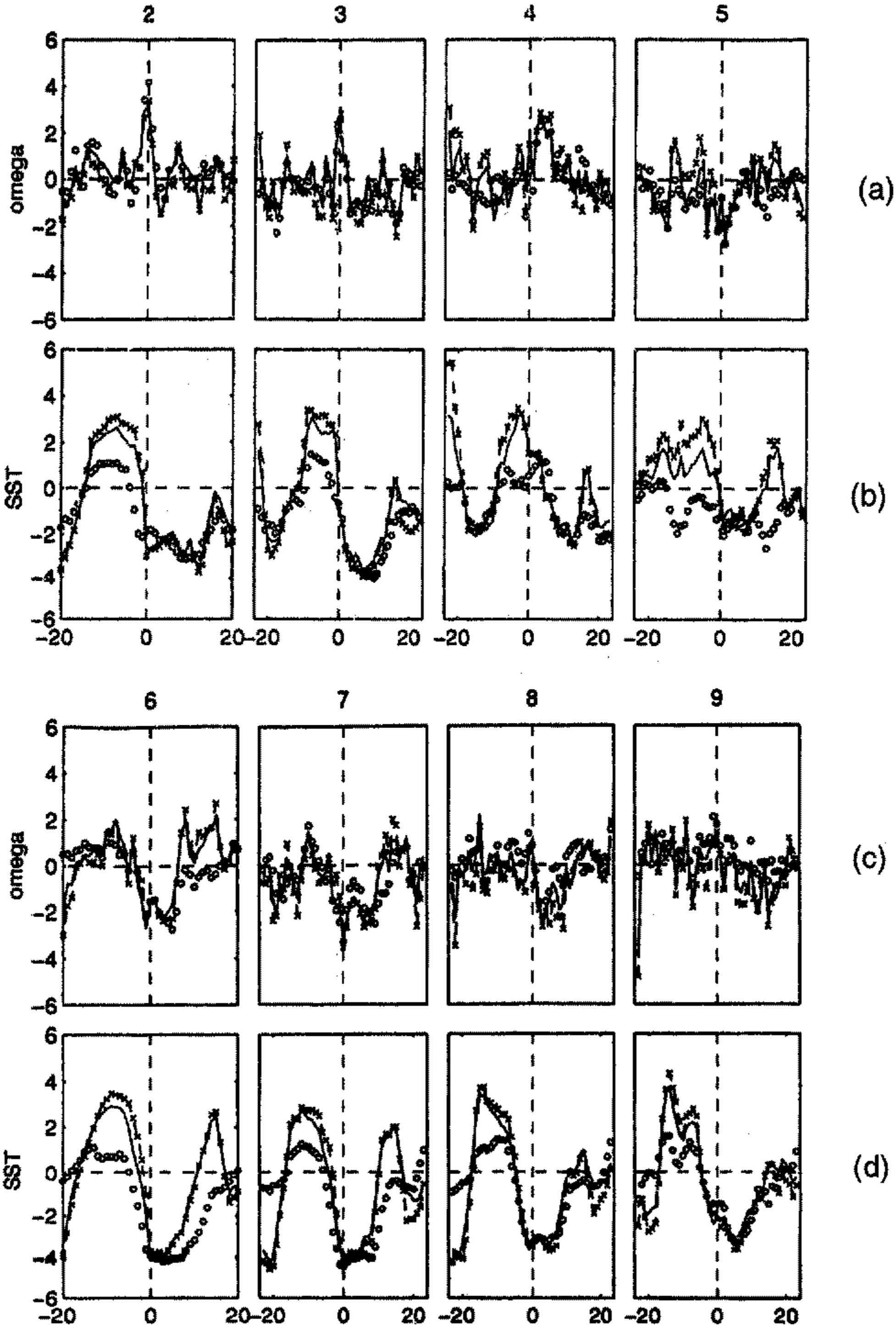

Figure 6. Lag correlations (×10) (general-circulation model variables) between (a) and (c) Indian monsoon rainfall for July–September (IMR(JAS)) and vertical velocity, and (b) and (d) IMR(JAS) and sea surface temperature (SST), along the equator from the Indian to Pacific Ocean, i.e. boxes 2-B to 9-B in Fig. 4. The original correlations are shown by small circles, while the correlations based on type II elimination are shown by the solid line (threshold of 0.05 to define type I/type II) and the cross-dashed line (0.09 threshold). x-axis is lag in months.

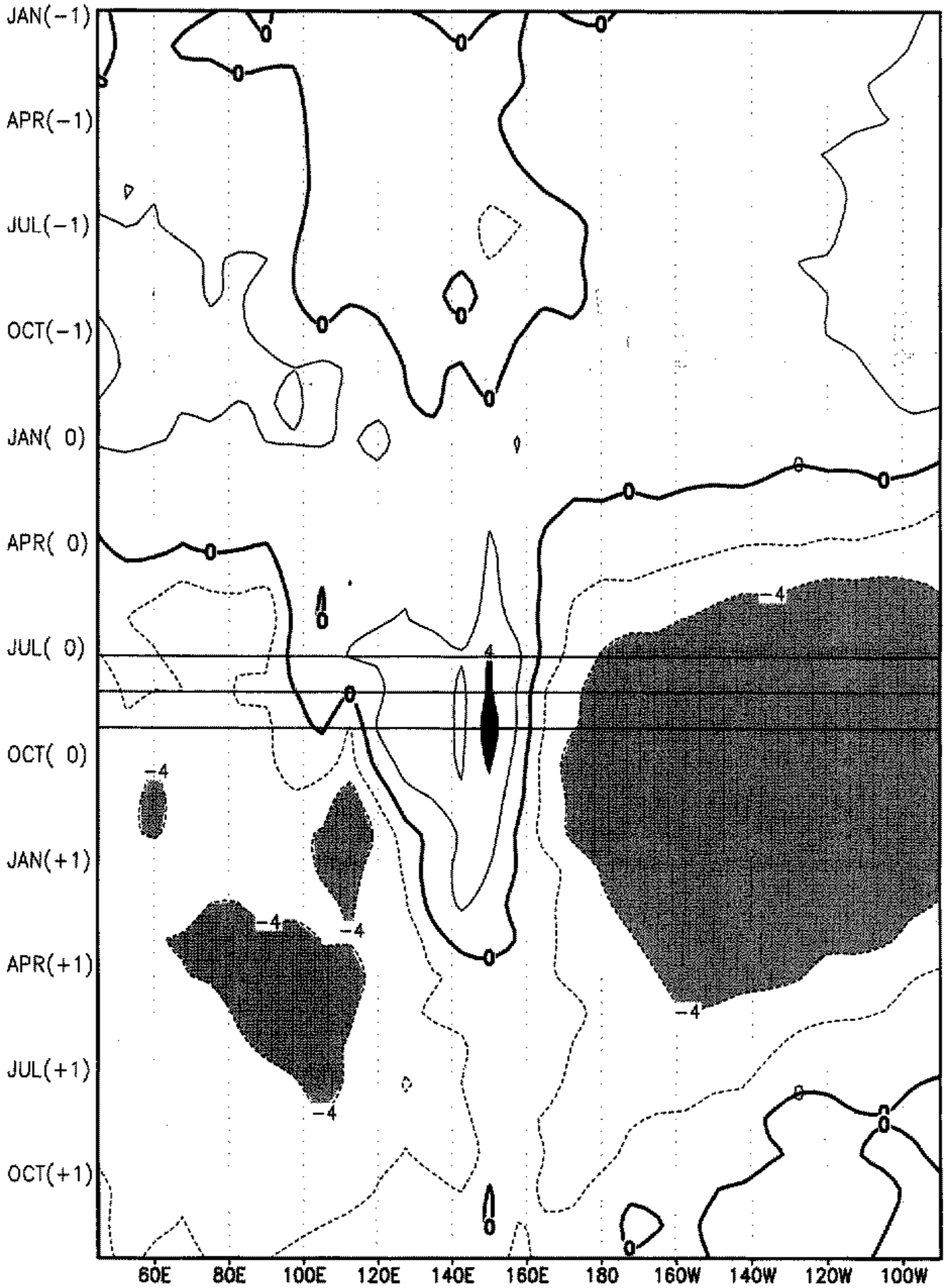

Figure 7. Longitude–time diagram of lag correlation (×10) for the model's Tropical-wide Oscillation Index for July–September (TOI(JAS)), and the sea surface temperature anomalies over the 10°N–10°S belt along the Indo-Pacific longitudes. The ordinate is the lead or lag time from January (−1) (top) to December (+1) (bottom). The TOI(JAS) is referred to the middle of the ordinate, i.e. JAS(0) at which three lines are drawn. Contour interval is 2. The areas less than −4 are light shaded, and those greater than 4 are dark shaded.

for obtaining an overall view of the time sequence. In this respect, time–longitude sections of lag correlations have an advantage, as used by Y90 and SL95.

Figure 7 shows the correlation between the model TOI(JAS) and observed SST anomalies along the equatorial Indo-Pacific Oceans (10°N–10°S). The abscissa is longitude and the ordinate time, from −1 to +1 year, centred around the host season

JAS(0) for the TOI (see the three horizontal lines). Correlation levels above the three lines represent precursory signals from the SST to the TOI(JAS), while the lower part represents precursory signals from the TOI(JAS) to the ENSO. The correlations are appreciably larger in the positive time domain, from 0 to +1 year.

The pattern of Fig. 7 closely resembles that of SL95 (see their Fig. 10), despite a different host variable, i.e. the Eastern Asian monsoon in the case of SL95. This is quite plausible, because the IMR(JAS) and the Eastern Asian summer monsoon are similar to each other in terms of timing of the phenomena (2 ~ 3 month difference). Figure 7 is also consistent with Verma (1994), who noted a reversal in correlation sign from positive to negative, as the seasons progress from boreal winter through March–April–May (MAM(0)).

Similar diagrams to Fig. 7 but for omega at the 500 hPa level over India are calculated. The latitude of this new strip is denoted as the C′-latitude, i.e. 15°N–30°N, shifted slightly northward from the C-latitude (Fig. 4), so that the Indian subcontinent is fully included in the target region. Figure 8 is the lag correlation of omega in the C′-latitude with the TOI(JAS). The three model omegas are target variables. One of the noteworthy points is the similarity of this diagram to that for SST (Fig. 7) over the longitudes of the Pacific Ocean but again not over the Indian Ocean. The correlation patterns of omega are smoothly connected between the Indian and the Pacific sectors. This is quite reasonable, because omega reflects the SST in the Pacific, and yet the atmosphere is spatially well mixed, compared with the ocean.

(*b*) *Utility of the TOI(JFM)*

We have investigated the lead–lag properties of the TOI and ENSO–monsoon system, taking only the season of JAS as host, so we now turn to the TOI(JFM). Figure 9 is a diagram of correlation between the model's TOI(JFM) and omega anomalies for all months. A noteworthy point is that the correlation patterns for JFM are similar to those for JAS, except that the host index is located at JFM(+1) (three horizontal lines).

One of the critical questions is whether the TOI(JFM) is effective in serving as a teleconnection index involving lag correlations with the Indian monsoon. Figure 9 is compared with the TOI(JAS) (Fig. 8). Figure 8 is characterized by a positive correlation at July(0), 70°–80°E, corresponding to the Indian summer monsoon, and by the negative correlation at July(0), 150°–140°W over the eastern Pacific. On the other hand, Fig. 9 is characterized by a positive correlation pole at JFM(+1) over 160°E–160°W, east of the Z-region, and another positive pole over India at JAS(0), 60°–90°E. However, a most critical question is whether a strong signal can be found at JAS(+1) over the Indian sector (60°E–90°E). The answer is no. A similar diagram to Fig. 9 is made, based on the TOI(JFM) of Xie–Arkin and the target variable, omega, of ERA (not shown). The result appears to support the model's result (Fig. 9). Thus it is concluded that the TOI(JFM) has no precursory signal for the Indian monsoon for the following summer. The result described here is consistent with the original reports of Walker (1936) who found his boreal winter SOI of little use for the prediction of Indian summer monsoon rainfall.

So far, we have been unable to find additional information on the ENSO–monsoon system by using the TOI(JFM). It has been discussed, however, that the East Asia winter monsoon could be an important element to trigger the ENSO (for example, Chang and Lau 1982; Y90; Zhang *et al.* 1997; Meehl 1997), and that the SST in this region is influenced by the north-east winter monsoon and the Australian monsoon, and these monsoons may play an important role in the formation of the biennial or

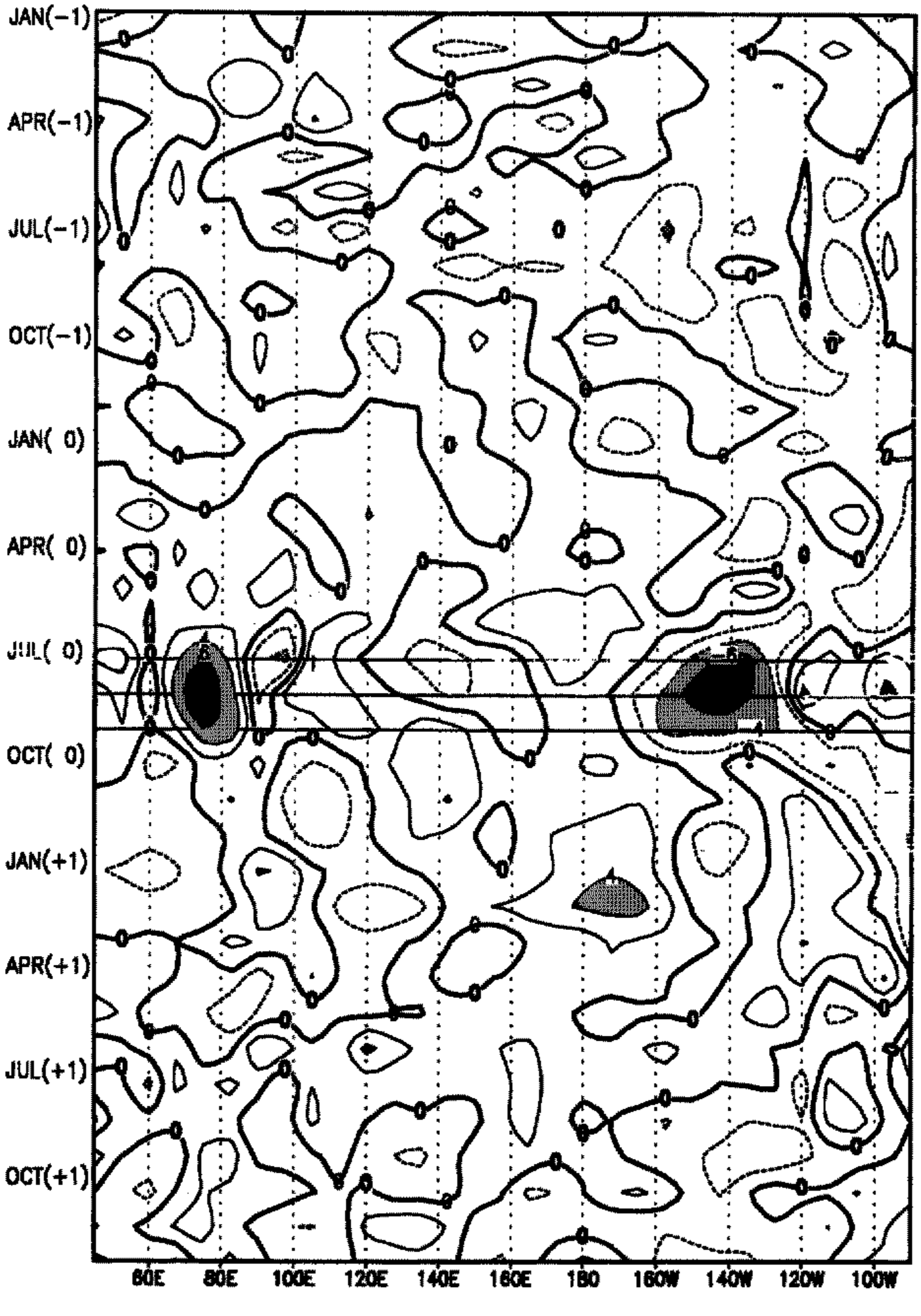

Figure 8. The model's Tropical-wide Oscillation Index for July–September (TOI(JAS))–vertical-velocity (omega) correlation, omega being at the C′-latitude, i.e. 15°–30°N. The omegas used here are the model results. See the caption of Fig. 7 for details.

quasi-biennial oscillation (Masumoto and Yamagata 1991; Tomita and Yasunari 1993). As Meehl (1987) and Murakami and Wang (1993) note, the convective maximum and large-scale east–west linkages between Indian and Pacific sectors have a diagonal north-west to south-east character, not a simple north–south (regional Hadley) or east–west relationship.

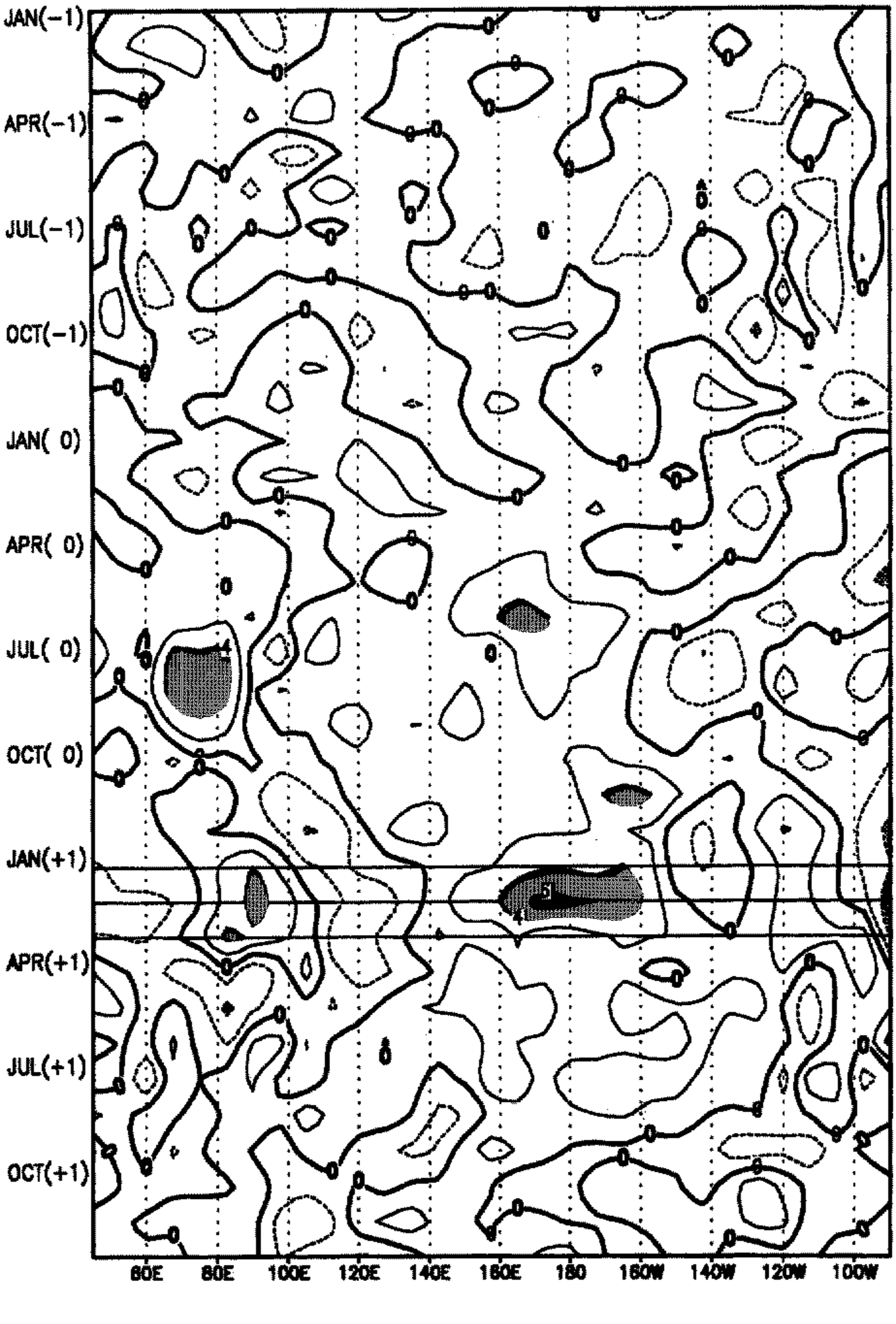

Figure 9. The same as Fig. 8 but the host variable is the model's TOI for January–March.

6. TYPE I AND TYPE II STATES

We will now turn to the second index for the separation of type I/type II states. As explained by the analogy of the swing, section 2(b), we examine which case corresponds to the strongly pulled swing and which corresponds to the equilibrium swing.

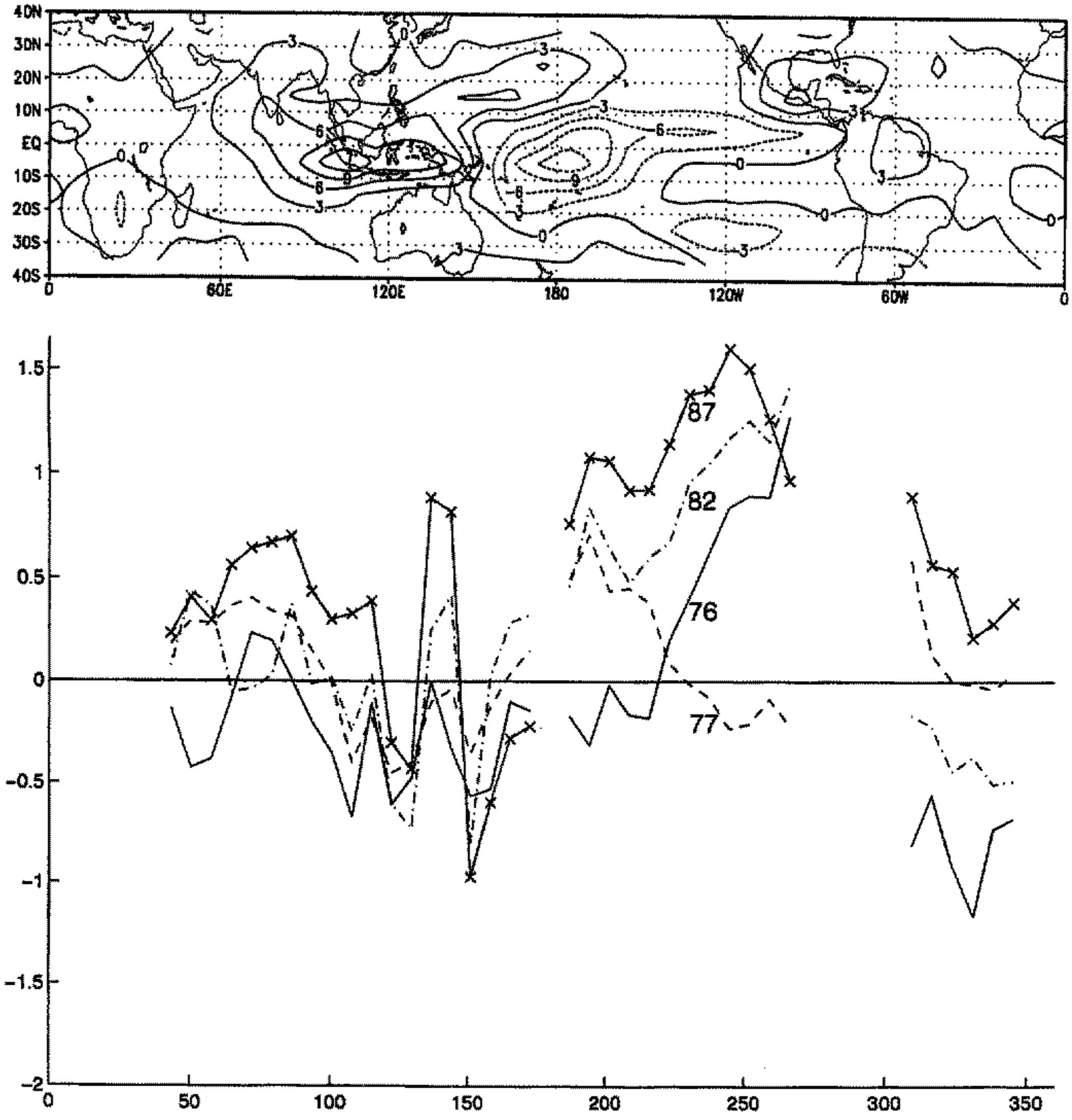

Figure 10. The longitudinal distributions of sea surface temperature for July–September (SST(JAS)) anomalies (degC) in the 0°–10°S belt for (a) the type I-east years, (b) the type I-west years, and (c) the type II years (lower panels), together with the composite outgoing long-wave radiation (OLR) anomalies (upper panels). For OLR the contour interval is 3 W m^{-2}, with the positive and negative contours being solid and dashed lines, respectively.

(*a*) *OLR and SST*

The negative/positive regions of the OLR distribution may represent the convectively active/benign areas. Figures 10(a), (b) and (c) are composite maps of observed OLR anomalies (upper panels) along with the corresponding individual observed SST anomaly profiles (lower panels) for the latitudinal band of 0°–10°S. In these figures the results for JAS only are shown, because the patterns are clearer for JAS than those for MAM, for example. Based on all cases of JAS from 1975 to 1993, a total of four composite groups are identified. The method of classification will be explained in subsection 6(b). The four groups are: type I-east (Fig. 10(a)) in which the absolute SST

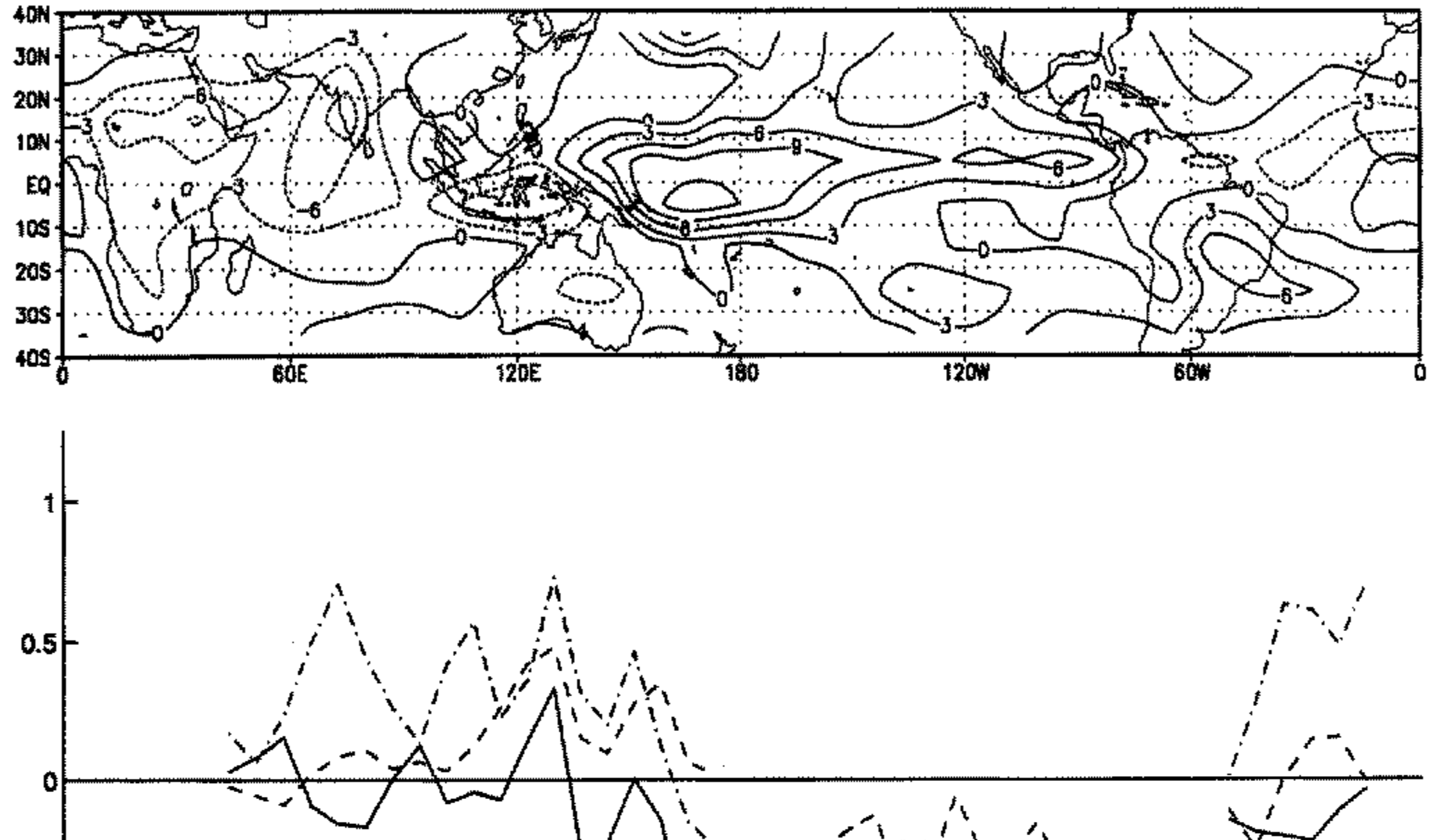

Figure 10. Continued.

maximum (not anomaly) is located east of 180°; type II-east (Fig. 10(c)) in which the maximum of SST is between 170°E and 180°; type II-west (not shown here) in which the maximum is between 160°E and 170°E; and type I-west (Fig. 10(b)) in which the maximum is located west of 160°E. For example, the years 1976, '77, '82 and '87, two of which are El Niño years, belong to type I-east; and generally most La Niña years belong to type I-west.

The location of the minimum in negative OLR anomaly clearly shifts longitude with each sub-group of years. It is interesting to point out that the positive/negative anomaly centres along the equator appear as a dipole, being located closely side by side, indicating that the Walker circulation is slightly shifted eastward or westward from its normal position. A most intriguing aspect is that in Figs. 10(a) and 10(b) (type I) the OLR anomalies are spread over a wide area even off the equator, particularly over the Indian subcontinent, while in Fig. 10(c) the OLR anomalies tend to be confined to a small region, the warm-pool, around New Guinea along the equator. In other words, the Walker circulation is mostly confined along the equator, in type II, but in the type I case

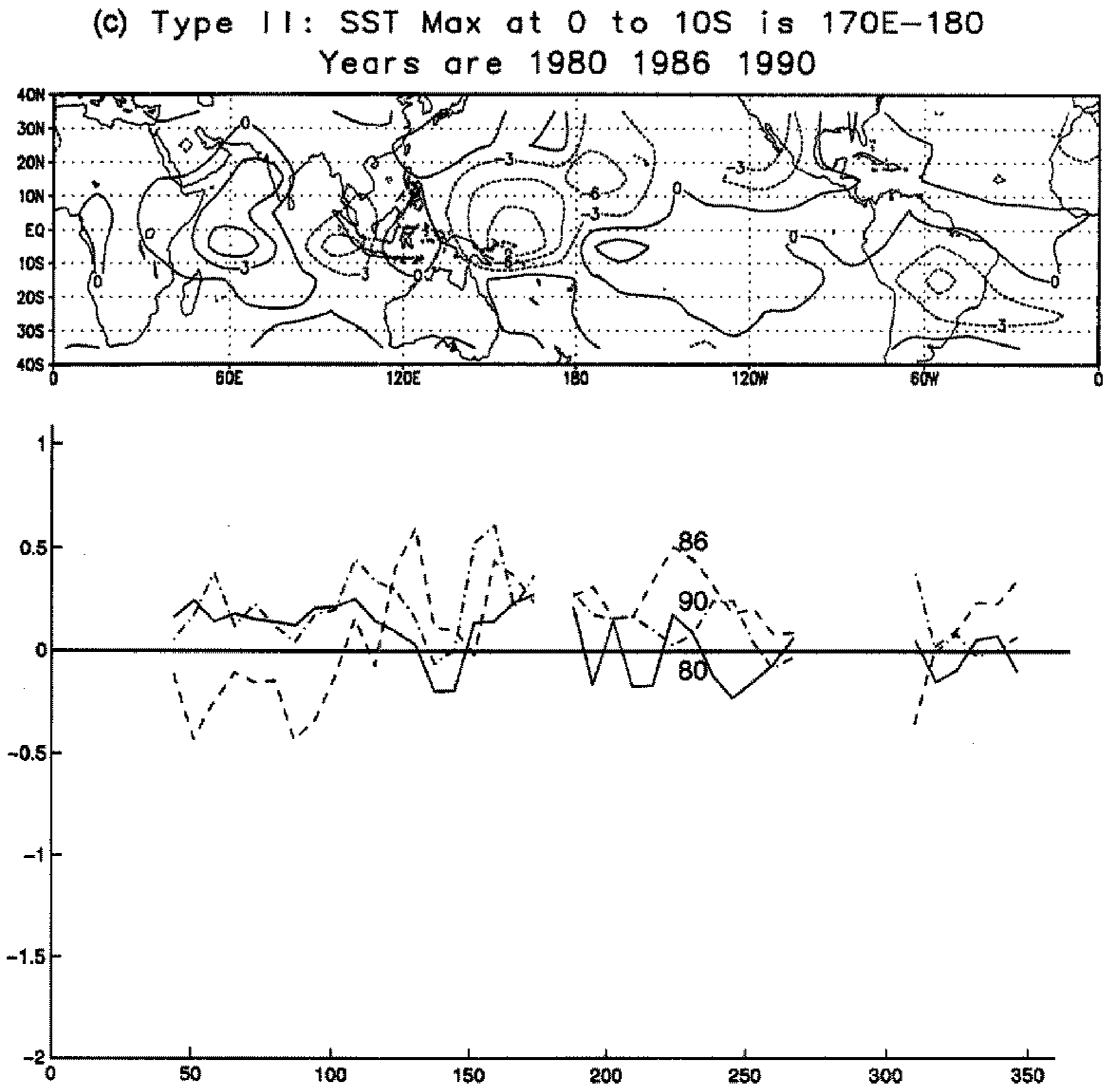

Figure 10. Continued.

the associated vertical-velocity anomaly areas are widely distributed off the equator, i.e. particularly over India, Sahel and South America (Fig. 10(a)) and over India, China, and subtropical North and South Pacific (Fig. 10(b)).

Nigam (1994) studied the dynamics of the Asian summer monsoon rainfall–El Niño linkage through diagnostic calculations with a linear steady-state primitive-equation model. It is interesting to note that the OLR anomaly pattern he used (his Fig. 1(a)) is very similar to that of Fig. 10(a)) in this paper, because he took the difference of JJA OLR between 1987 and 1988 (El Niño year minus La Niña year). With this heating, he calculated the three-dimensional flow patterns, using the linear model. He then obtained a strikingly similar pattern to the observation for the June–August circulation near the surface and in the upper atmosphere. In other words, the case of type I-east (or type I-east minus type I-west) has a dynamical connection between the ENSO and Indian rainfall. This indicates that the hypothesis on the pendulum of the Walker circulation–the Indian monsoon is not consistent with the linear steady-state dynamics. It is likely, therefore, that the case of type II has no connection between the ENSO and the Indian rainfall.

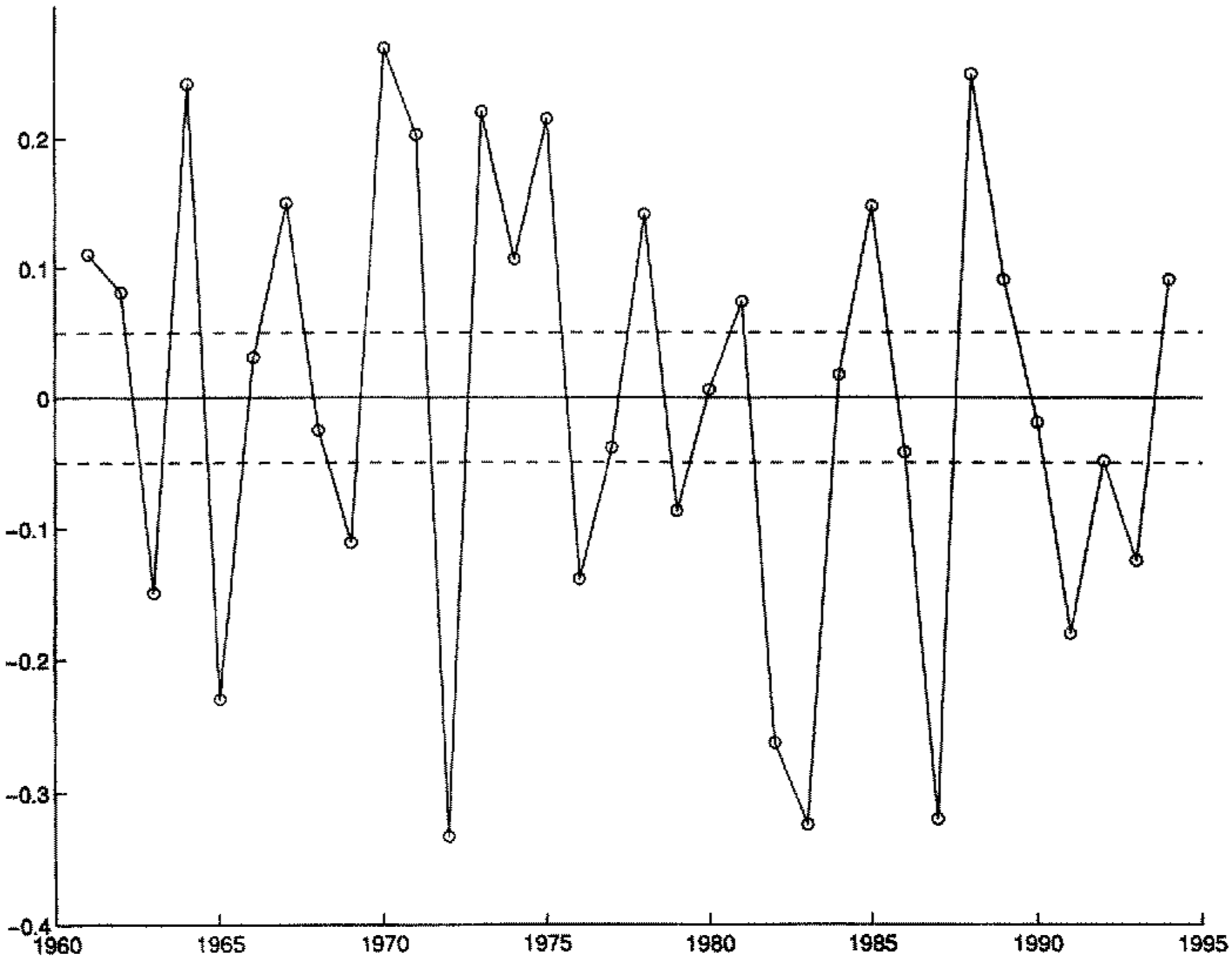

Figure 11. Time series of the Walker circulation Index, i.e. time coefficients of the empirical orthogonal function mode 1 of the normalized sea surface temperature anomalies in the 0°–10°S belt in the equatorial Indo-Pacific from 45°E to 82°W. The dashed lines are for $\varepsilon = -0.05$ (see text); the small circles between these dashed lines are categorized as type II years.

(*b*) *Separation of type I/type II years*

The determination of the type I/type II years is now performed in a more precise way. The longitudinal distribution (45°E–180°–82°W) of SST anomalies along the latitudinal belt of 0°–10°S, such as in Fig. 10, are taken, and a correlation EOF analysis is applied to the anomalies. (In fact, an EOF analysis confined to the Pacific Ocean (135°E–82°W) does not change the results reported later.) The 34-year series of the EOF time coefficients is shown in Fig. 11. The EOF 1 accounts for about 62% of the total variance, while EOF 2 and 3 account for about 10% each. Therefore, the first mode alone (EOFSST) can represent the equatorial Indo-Pacific SST profile fairly well.

The longitudinal distribution of EOFSST (not shown) resembles closely the SST anomaly profiles in Fig. 10(b) and (reversed sign) Fig. 10(a). There is a very strong gradient of weights from approximately 0.6 (near 115°E) to −0.6 (near 175°E). Type I years will be those with large amplitude (either positive or negative) when projected on EOFSST. It is hypothesized here that type I years have a spatially extensive teleconnection capability from one location to another, particularly between ENSO and Asian monsoons. On the other hand, type II years have no teleconnection or only localized effect. From this point on, this hypothesis will be examined in various ways.

The next question is: what is the most reasonable threshold value for the determination of type I/type II? The dashed lines in Fig. 11(a) mark a 0.05 threshold. This threshold is chosen arbitrarily at this point, except that the classification almost exactly

agrees with the subjective specification based on the longitudinal profile of the SST. The cases above 0.05 are type I-west, those below −0.05 are type I-east, and the cases between are categorized as type II. With this classification, there are 26 cases for type I and 8 cases for type II. If the threshold is changed to 0.1, the ratio changes to 22 for type I and 12 for type II. In short, the type II state is defined as those years in which the Walker circulation is close to the climatological normal.

(*c*) *Timing of the phase change*

Another question about the timing of the phase is whether JAS is the right season for determining the bifurcation. For example, could MAM or JFM be better? In particular MAM has been considered as the starting season for new biennial oscillations. Also what is the duration of type II? In order to examine these aspects, the seasonal variation of SST anomalies along the equatorial Indo-Pacific Ocean (0°–10°S, 45°E–82°W) was investigated by calculating EOFs of the SST-profile for each season.

The loading (space) functions for EOF 1 in the different seasons are quite similar to each other except for the strength of gradient across 160°E (not shown). They are characteristically divided into the left and right longitudes around 160°E, corresponding to (i) dominantly the Indian Ocean (moderate negative weights) and western Pacific (positive weights of large magnitude) and (ii) dominantly the central/eastern Pacific Ocean (negative weights). The longitudinal gradient across 160°E is largest in JAS and smallest in JFM. Figure 12 shows the seasonal variation of the time coefficients of EOF 1 for different years. The abscissa is the season from JFM to September–October–November (SON). There are three panels: the left is for the years of type I of $|\mathrm{EOF(JAS)}| > 0.15$, the middle is for type I of $0.15 > |\mathrm{EOF(JAS)}| \geq 0.10$, and the right is for type II. These figures may indicate that for clear type I cases, MAM (EOF 1 is 60% of total variance) is the starting (wash-out) season; the characteristic feature of the curve is being established in May–June–July (MJJ); the curve in JAS (62%) is a continuation from the previous season; and that of SON (75%) is at its mature stage, except that the curve for 1983 in the left panel is exceptional; it is not stable in JAS.

Therefore, the best time for identifying type I/type II may be JAS, though it is too late for summer monsoon prediction. On the other hand, MAM may be too early for determining the types. In this paper we choose JAS, because the main objective of this paper is not to forecast. The duration of type II is about 4 months, i.e. from MJJ to SON; after SON, there is a transition and the growth or decay of EOFSST occurs in MAM if the new year is to be a type I (not shown). In the study of ENSO forecasts (Cane and Zebiak 1985), it is considered that MAM is the season of 'spring barrier', in which forecasts at the equator become chaotic. Wright (1985) and Trenberth and Shea (1987) also state that the transition of the SOI occurs mostly around MAM. For the same reason, the validity of TOI(JFM) for the host variable is questioned, because JFM is before the chaotic boreal spring season. In summary, it may be reasonable to adopt EOFSST for JAS; it is denoted by WAI(JAS) (Walker circulation Index) or simply WAI and subsequent analyses will show it to be a good indicator of type for the year (an exception is for 1983).

(*d*) *Equatorial teleconnection excluding type II cases*

The solid lines and the cross-dashed lines in Fig. 6 (shown earlier) are the results of type II elimination. The hypothesized threshold in this paper is 0.05, though this value has been experimentally varied and some results from other thresholds are shown. Whenever type II appears, the correlation sequence is terminated and re-opened after

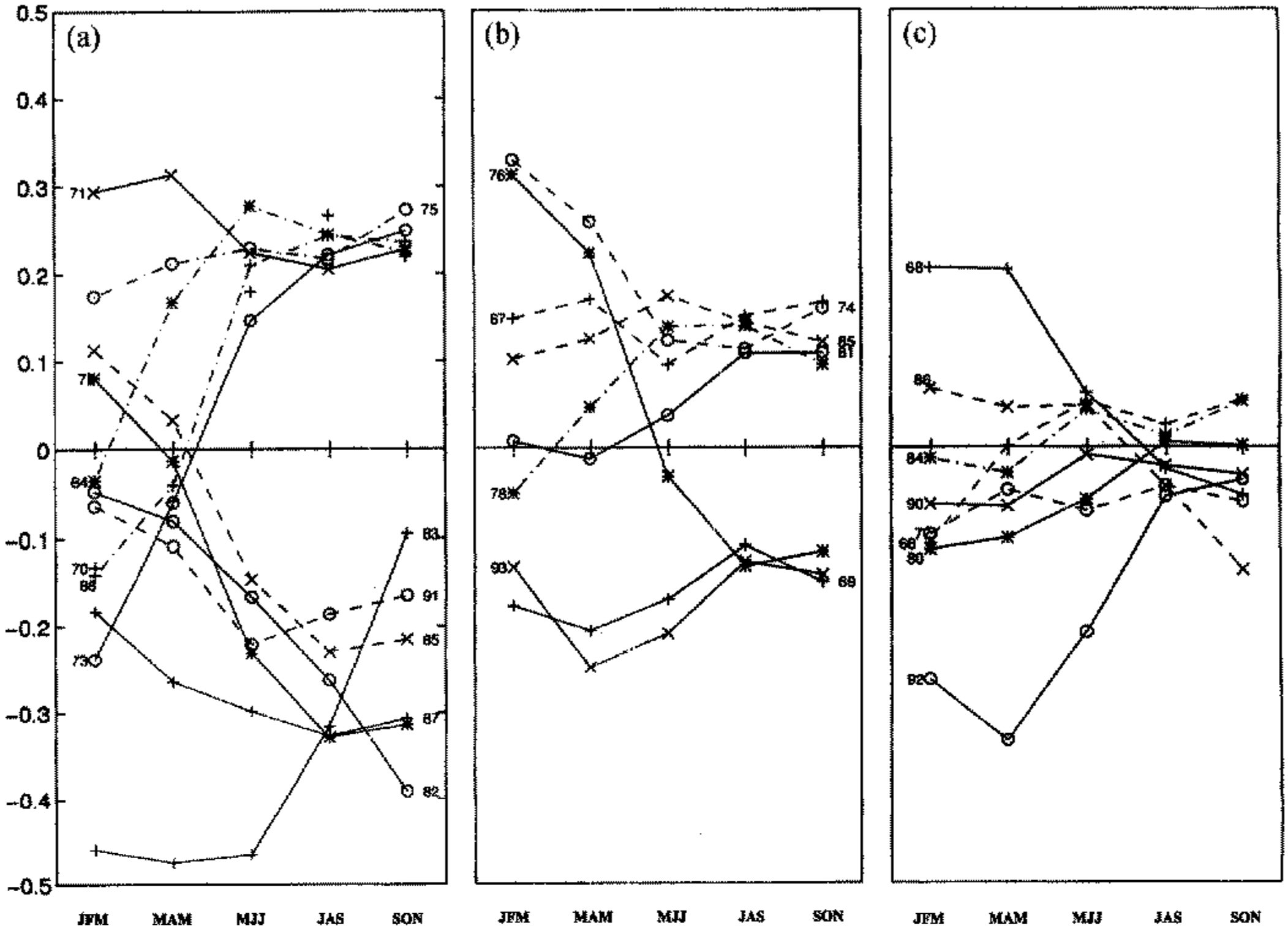

Figure 12. The evolution in individual years of the time coefficients of the empirical orthogonal function (EOF) mode 1 of normalized sea surface temperature (SST) anomalies along the equatorial Indo-Pacific. The abscissa is the time of year (season), and the ordinate is the time coefficient value. (a) The cases (years) belonging to extreme type I, |EOFSST| for July to September (JAS) larger than 0.15; (b) the cases (years) belonging to moderate type I, |EOFSST| for JAS between 0.15 and 0.10; and (c) the cases (years) belonging to type II.

the extended type II is over. Furthermore, in the lag-correlation diagrams, the type II disruption should not be present in either of the two consecutive years. This constraint is applied to positive and negative (lagged and lead) time coordinates separately. The results of two thresholds are shown in Fig. 6, i.e. 0.05 and 0.09. There are eight type II years out of 34 years with the 0.05 criterion, while there are ten type II years with 0.09 (not shown). It is seen in Fig. 6 that the removal of extended type II increases correlations appreciably. Perhaps the most important improvement is in the negative time ordinate for SST, where positive correlations in the Indian Ocean and central and eastern Pacific are inflated, exaggerating the transition from positive correlations a few months before the host JAS season, to negative correlations during and after the host season. Recall that these diagrams are the average of nine correlation profiles using separately as host index the monthly IMR in July, August and September in each of the three runs.

It is natural to ask whether other indices can be used to determine type I/type II states with equal or better success in focusing on ENSO–monsoon interaction. We tried various other indices, always selecting the threshold so as to define type II to occur in about eight years out of the 34 years. Using EOF 1 of the SST profile 0°–10°N, 45°E–82°W gave only three type II cases in common with the earlier classification, and lag correlations with ENSO–monsoon parameters were only marginally improved in type I years. Using the SOI gave five type II years out of eight, in common with the earlier classification. With the SOI classification, lag correlations in type I years were amplified somewhat in the positive time domain, but not in the negative time domain. In

TABLE 1. VARIOUS INDICES BASED ON OBSERVED DATA FOR ALL YEARS FROM 1961 TO 1994. FOR FURTHER EXPLANATION SEE SECTION 6(e).

Year ε	IMR 0.6	TOI/X–A 0.6	TOI/CRU 0.6	SOI 0.6	EST −0.8	WAI 0.15	Type 0.05
1961	0.84 P		0.42	−0.08	0.03	0.11	Iw
1962	0.17		0.07	0.28	−0.82 P	0.08	Iw
1963	−0.50		−0.33	−0.46	1.17 N	−0.14	Ie
1964	0.92 P		1.22 P	1.33 P	−1.79 P	0.24 P	Iw
1965	−1.00 N		−1.67 N	−1.65 N	1.53 N	−0.23 N	Ie
1966	−1.13 N		−0.35	0.19	0.43	0.03	II
1967	1.20 P		0.51	0.54	−0.26	0.14	Iw
1968	−1.02 N		−0.39	0.17	0.22	−0.02	II
1969	0.25		0.07	−0.85 N	0.75	−0.11	Ie
1970	1.20 P		1.02 P	0.28	−1.13 P	0.26 P	Iw
1971	−0.02		0.27	0.95 P	−0.76	0.20 P	Iw
1972	−1.90 N		−2.42 N	−1.93 N	2.30 N	−0.33 N	Ie
1973	0.27		0.73 P	0.72 P	−1.37 P	0.21 P	Iw
1974	0.05		0.25	0.64 P	−0.51	0.10	Iw
1975	1.55 P		1.42 P	2.00 P	−1.21 P	0.21 P	Iw
1976	−0.16		−1.04 N	−1.56 N	0.73	−0.13	Ie
1977	−0.65 N		−0.53	−1.31 N	0.95 N	−0.03	II
1978	−0.09		0.66 P	0.42	−0.19	0.14	Iw
1979	−0.21	0.57	−0.26	0.56	−0.03	−0.08	Ie
1980	−0.57	−0.26	−0.13	0.01	0.15	0.00	II
1981	1.00 P	0.86 P	0.75 P	1.05 P	−0.78	0.07	Iw
1982	−0.82 N	−1.03 N	−1.09 N	−2.02 N	1.29 N	−0.26 N	Ie
1983	1.90 P	−0.39	0.27	0.44	−0.24	−0.32 N	Ie
1984	−0.52	0.62 P	0.01	0.42	−0.77	0.01	II
1985	−0.96 N	0.38	0.57	0.41	−0.46	0.14	Iw
1986	−0.23	−0.67 N	−0.82 N	−0.26	0.59	−0.04	II
1987	−1.24 N	−1.17 N	−1.80 N	−1.54 N	1.95 N	−0.32 N	Ie
1988	2.54 P	1.56 P	2.63 P	1.72 P	−1.64 P	0.24 P	Iw
1989	−1.22 N	0.51	0.24	0.43	−1.22 P	0.09	Iw
1990	0.46	−0.22	−0.37	0.02	0.25	−0.01	II
1991	−0.84 N	−0.43	−0.81 N	−0.44	0.46	−0.18 N	Ie
1992	0.36	0.09	0.11	0.60 P	0.11	−0.04	II
1993	−0.78 N	−0.27	−0.65 N	−0.23	−0.23	−0.12	Ie
1994	0.72 P	−0.09	1.40 P	−0.86 N	0.51	0.09	Iw

summary, of the indices we considered, the SST EOF for the southern equatorial Indo-Pacific profile (Fig. 11) was the most successful in defining type I years which focus on ENSO–monsoon lagged interaction.

In section 2(b), another method was mentioned, i.e. the localized heat source associated with the ENSO. Concerning this method, a discussion will be given in Part II, focusing on the ENSO–monsoon relation.

(*e*) *Table of the observed indices*

Table 1 shows the 'time coefficients' of the TOI and other indices. The indices are all for JAS. TOI/X–A in the third column is the TOI(JAS) obtained from the Xie–Arkin data, and the TOI in the fourth column is obtained from the CRU rainfall data (land stations, therefore covering continental and island regions), that will be denoted in the following as TOI/CRU. Researchers at the UK Meteorological Office have advocated an index of the Sahel rainfall for (JAS) to describe the tropical-wide teleconnection, though many papers (e.g. Nicholson 1979; Janicot *et al.* 1996) have mentioned that the major time-scale of Sahel drought variation is much longer (decadal) than that of the ENSO. In other words, a different mode is probably included. To focus on the

ENSO time-scale, the decadal variability was removed from the TOI/CRU by applying an integrated random-walk Kalman filter with a 50% cut-off amplitude set to 11.25 years. This filter was also applied to all the JAS host indices in Table 1, though it is only critical for studies involving SahelR (JAS), and similar results for TOI/CRU are found using filtered and unfiltered versions of the time series. The SOI is the Tahiti minus Darwin SOI for JAS (raw data provided by R. Allan (1996), personal communication). The EST is defined as the normalized JAS SST in the central equatorial Pacific (10°N–10°S, 180°W–150°W, i.e. Box 6-B (Fig. 4) (close to NINO3 SST). EST will be used for the test of a localized heat source in Part II (Miyakoda *et al.* 1999). On the other hand, the separations of type I/type II based on JAS are shown in the column headed WAI. The last column is the separation of type I-east (Ie), type I-west (Iw), and type II, based on the WAI in the previous column. It may be interesting to compare WAI with SOI. P and N in Table 1 indicate the outstanding positive and negative values, respectively, for a specified threshold (note that for the EST, the threshold is set to the opposite sign $\varepsilon = -0.8$, because of convenience for comparison). The 'agreement' between the two indices is defined here as follows. If two indices for the same year show P–P or N–N, they are regarded as 'in agreement'.

(1) The TOI/CRU and the SOI are quite similar, ten agreements out of 20 outstanding cases. Correlations are 0.87 (0.90) without (with) type II separation. The independent information in the TOI/CRU is therefore small, but nonetheless important for ENSO–monsoon lead–lag studies.

(2) Good correspondence is found between the SOI and the EST, and also between the TOI/CRU and EST, i.e. both have nine agreements out of 20 outstanding cases. The correlations are also calculated using all values of the indices. Correlations are –0.87 and –0.82 for the former and the latter couples, respectively. The SOI represents the EST slightly better than the TOI/CRU.

(3) There are 12 agreements out of 24 outstanding cases between the TOI/CRU and IMR, compared with nine agreements out of 25 outstanding cases between the SOI and IMR. Correlations are 0.79 and 0.65 without type II separation, respectively, while they are increased to 0.82 and 0.70 with separation. This indicates that the TOI/CRU is closer to the IMR than the SOI is to the IMR. This fact may support the concept that the TOI/CRU embraces both the IMR and the SOI and, therefore, it may represent better the ENSO–monsoon system.

(4) Concerning the Indian summer monsoon rainfall, Parthasarathy *et al.* (1987) noted that the worst droughts occurred during 1965 and 1972, and the worst floods in 1961 and 1983. Obviously they are represented well by the IMR. The TOI/CRU(JAS) and SOI(JAS) agree with the two drought cases. The TOI/CRU(JAS) is moderately positive for the flood cases whereas the SOI(JAS) is of the wrong sign for the 1983 flood.

(5) The TOI/CRU(JAS) appears to have a tendency toward a biennial periodicity if type II years are eliminated. Focusing only on consecutive type Is in Table 1 and with the threshold $\varepsilon = 0.05$, it is possible to see that the TOI/CRU index values tend to alternate between positive and negative. With the notable exception of only two periods (1962 and around 1971), with a more tightened criterion ($\varepsilon = 0.10$) for type I classification, only one case (1971) remains.

(6) The TOI/X–A is compared with the TOI/CRU. This comparison may provide an interesting and crucial test on the robustness of TOIs because both TOIs are obtained from quite different sources. Comparison of the two sets of time series reveals that there

are five agreements out of nine outstanding cases, and that the correlation is 0.84. This degree of agreement is satisfactory.

(7) Investigation based on a 42-year series of data (Ward, personal communication) revealed that this TOI/CRU(JAS) is positively correlated (0.61) with SahelR (JAS).

To summarize, the TOI/CRU, the IMR and the SOI have common elements, and yet the TOI/CRU is closer to the IMR than the SOI. This lends support to the assumption that the TOIs are good for both phenomena over the tropical Pacific and Indian sectors and, therefore, the TOI/CRU(JAS) is a more appropriate index for the ENSO–monsoon system than the SOI or the IMR alone. Additionally, the TOI/CRU(JAS) appears to have a noticeable biennial periodicity for outstanding years with type II removed except the year 1971, and using TOI/CRU(JAS) as host index in lag correlations identified the biennial periodicity from JAS(0) to JAS(−1). The appropriateness of TOI/CRU(JAS) in terms of robustness is described in item (6) above. For the TOI, it appears that the most easily missed (by the GCM) important areas of precipitation for JAS are the Indian subcontinent and the NPCZ (near the Philippine Islands); even observations of precipitation are not satisfactory in the latter region.

7. Conclusions

Simulation of the Indian summer monsoon rainfall with a GCM is a delicate problem. It is very sensitive to the properties of a model, and the simulated rainfall areas are easily shifted from the observed areas. The main objective of this paper is to investigate the teleconnection characteristic for the ENSO and Asian monsoons, using the model's vertical velocity and rainfall. In practice, both model results and observation data are used extensively.

As an indicator of tropical teleconnection, the distributions of vertical velocity (omega) and rainfall are examined. The loading functions of EOF 1 of both variables are very similar to each other, and they show the geographical centres of these anomalies. Although the function covers the Pacific and Indian sectors, and possibly the African sector, the teleconnection centres of the anomalies migrate seasonally from the Indian subcontinent during JAS (region A) to the western Pacific in JFM (region Z). The teleconnection maps are characterized by the horseshoe pattern with the region A or Z at their western tips.

The time coefficient of the EOF mode 1 of precipitation is adopted as a teleconnection index, because the observation data of precipitation for 34 years are available (CRU data, for example) but not the observation data of omega. The EOF 1 of the precipitation is denoted as the Tropical-wide Oscillation Index (TOI). In principle, the indices for two seasons, i.e. TOI(JAS) or TOI(JFM), can be used as the tropical teleconnection indices. Judging from the correlation patterns of vertical velocity as well as precipitation, the TOI(JAS)'s strong influence domain is confined to the tropical region mostly around the eastern longitudes, particularly including the Indian subcontinent. On the other hand, the TOI(JFM)'s strong influence domain spans the whole Pacific Ocean, extending meridionally at least as far as 50°N. However, the domain does not cover the Indian longitudes.

Based on this preliminary study, the TOI(JAS) was chosen for the index which represents the strength of teleconnection between ENSO and Asian monsoons. This index is closely correlated with the Indian summer monsoon, the IMR (0.79), as well as the SOI (0.82). The correlation between the SOI and IMR is somewhat weaker (0.65). This implies that the TOI embraces both the SOI and the IMR and, therefore, the TOI

represents the teleconnections of the ENSO–monsoon better than either the SOI or the IMR alone.

A TOI is estimated by two almost independent sources of precipitation, i.e. the CRU station data (TOI/CRU) and the Xie–Arkin data set (TOI/X–A). The correlation of the 17-year series is 0.84; the degree of agreement is satisfactory, implying that this index is robust.

The second index proposed in this paper is the WAI. Based on this index, two tropical states are determined, i.e. type I and type II. In this teleconnection framework, it is hypothesized that the type I/type II separation is effective for the continuation/disconnection of the ENSO–monsoon cycle. The type II state is associated with a climatologically close-to-normal zonal gradient of the SST anomalies over the Pacific Ocean belt. On the other hand, the type I state corresponds to situations deviating from the climatological normal in the SST distribution. It is proposed that the separation is determined by the WAI, i.e. the EOF 1 time coefficients of the SST in the 10° latitudinal belt south of the equator in the Pacific. The best season for identifying type I/type II is JAS, because MAM, for example, can be considered as a starting season after a type II, or a transition season (from one type I phase to the opposite type I phase), and is not stable for determining the type. Type I years often correspond to intense El Niño or La Niña cases (see 1982–83, 1972–73), 1977, however, is not considered a type I year.

The consequence of the type I/type II hypothesis was shown in Fig. 6 and Table 1. The issue will be investigated further in Part II of this paper.

REFERENCES

Barnett, T. P. 1985 Variations near global sea level pressure. *J. Atmos. Sci.*, **42,** 478–501

Bengtsson, L., Arpe, K., Roeckner, E. and Schulzweida, U. 1996 Climate predictability experiments with a general circulation model. *Clim. Dyn.*, **12,** 261–278

Bhalme, H. N. and Jadhav, S. K. 1984 Southern Oscillation and its relation to the monsoon rainfall. *J. Climatol.*, **4,** 509–520

Bjerknes, J. 1969 Atmospheric teleconnections from the equatorial Pacific. *Mon. Weather Rev.*, **97,** 163–172

Cane, M. A. and Zebiak, S. E. 1985 A theory for El Niño and the Southern Oscillation. *Science*, **228,** 1085–1086

Chang, C. P. and Lau, K. M. 1982 Short-term planetary scale interaction over the tropics and the mid-latitudes. Part I: Contrast between active and inactive periods. *Mon. Weather Rev.*, **110,** 933–946

Folland, C. K, Palmer, T. N. and Parker, D. E. 1986 Sahel rainfall and worldwide sea temperature 1901–85. *Nature*, **320,** 602–607

Gibson, J. K., Kallberg, P., Nomura, A. and Uppala, S. 1994 'The ECMWF ReAnalysis (ERA) project—Plans and current states'. In Tenth international conference on numerical weather prediction. American Meteorological Society, Portland, Oregon, USA

Gordon, N. D. 1986 The Southern Oscillation and New Zealand weather. *Mon. Weather Rev.*, **114,** 371–387

Goswami, B. N. 1995 A multiscale interaction model for the origin of the tropospheric QBO. *J. Climate*, **8,** 524–534

Hulme, M. 1994 'Validation of large-scale precipitation fields in general circulation models'. Pp. 387–406 in *Global precipitation and climate change*. Eds. M. Desbois and F. Desalmans. NATO ASI Series. Springer-Verlag, Berlin

Janicot, S., Moron, V. and Fontaine, B. 1996 Sahel droughts and ENSO dynamics. *Geophys. Res. Lett.*, **23,** 551–554

Krishnamurti, T. N. 1971 Tropical east–west circulations during northern summer. *J. Atmos. Sci.*, **28,** 1342–1347

Lau, K.-M. and Li, M. T. 1984 The monsoon of East Asia and its global association—a survey. *Bull. Am. Meteorol. Soc.*, **65,** 114–125

Masumoto, Y. and Yamagata, T. 1991 Response of the western tropical Pacific to the Asian winter monsoon: the generation of the Mindanao Dome. *J. Phys. Oceanogr.*, **21,** 1386–1398

Meehl, G. A. 1987 The annual cycle and interannual variability in the tropical Pacific and Indian Ocean region. *Mon. Weather Rev.*, **115,** 27–50

1997 The South Asian monsoon and the tropospheric biennial oscillation. *J. Climate*, **10,** 1921–1943

Miyakoda, K., Navarra, A. and Ward, M. N. 1999 Tropical-wide teleconnection and oscillation. II: The ENSO–monsoon system. *Q. J. R. Meteorol. Soc.*, **125,** 2937–2963

Moron, V., Navarra, A., Ward, M. N. and Roeckner, E. 1998 Skill and reproducibility of seasonal rainfall patterns in the tropics in a GCM simulation with prescribed SSTs. *Clim. Dyn.*, **14,** 83–100

Murakami, T. and Wang, B. 1993 Annual cycle of equatorial east–west circulation over the Indian and Pacific Oceans. *J. Climate*, **6,** 932–952

Nicholls, N. 1984 Predicting Indian monsoon rainfall from sea-surface temperature in the Indonesian–North Australian area. *Nature*, **307,** 576–577

Nicholson, S. E. 1979 Pp. 173–200 in *The Sahara and the Nile.* Eds. M. A. J. Williams and H. Faure. A. A. Balkema, Rotterdam, the Netherlands

Nigam, S. 1994 On the dynamical basis for the Asian summer monsoon rainfall–El Niño relationship. *J. Climate*, **7,** 1750–1771

Oort, A. H. 1994 'Global atmospheric circulation statistics, 1958–1973'. NOAA Professional. Paper 14

Parker, D. E. and Folland, C. K. 1991 'Global ocean surface temperature atlas: a presentation'. Pp. 225–230 in Proceedings of the NOAA 15th annual climate diagnostics workshop. October 1990, Ashville, NC, USA

Parthasrathy, B., Sontakke, N. A., Monot, A. A. and Kothawale, D. R. 1987 Droughts/floods in the summer monsoon season over different meteorological subdivisions of India for the period 1871–1984. *J. Climatol.*, **7,** 57–70

Pazan, S. and Meyers, G. 1982 Interannual fluctuations of the tropical Pacific wind field and Southern Oscillation. *Mon. Weather Rev.*, **110,** 587–609

Philander, S. G. H. 1990 *El Niño, La Niña, and Southern Oscillation.* Academic Press, Inc., San Diego, USA

Rasmusson, E. M. and Carpenter, T. H. 1982 Variations in tropical sea surface temperature and surface wind fields associated with the Southern Oscillation/El Niño. *Mon. Weather Rev.*, **110,** 354–384

1983 The relationship between the eastern equatorial Pacific sea surface temperatures and rainfall over India and Sri Lanka. *Mon. Weather Rev.*, **111,** 517–528

Rayner, N. A., Horton, E. B., Parker, D. E., Folland, C. K. and Hackett, R. B 1996 'Version 2.2 of the global sea-ice and sea surface temperature data set, 1903–1994'. Climate Research Technical Note No. 74, Hadley Centre for Climate Prediction and Research, Bracknel, UK

Rodwell, M. J. and Hoskins, B. J. 1996 Monsoons and the dynamics of deserts. *Q. J. R. Meteorol. Soc.*, **122,** 1385–1404

Roeckner, E., Arpe, K., Bengtsson, L., Christoph, M., Claussen, M., Dumenil, L., Esch, M., Giorgetta, M., Schlese, U. and Schulzweida, U. 1996 'The atmospheric general circulation model ECHAM-4: model description and simulation of present-day climate'. Report number 218. MPI, Hamburg, Germany

Shen, S. and Lau, K.-M. 1995 Biennial oscillation associated with the East Asian summer monsoon and tropical sea surface temperatures. *J. Meteorol. Soc. Japan*, **73,** 105–124

Shukla, J. and Paolino, D. A. 1983 The Southern Oscillation and long-range forecasting of the summer monsoon rainfall over India. *Mon. Weather Rev.*, **111,** 1830–1837

Sperber, K. R. and Palmer, T. N. 1996 Interannual tropical rainfall variability in general circulation model simulations associated with the Atmospheric Model Intercomparison Project. *J. Climate.*, **9,** 2727–2750

Tomita, T. and Yasunari T. 1993 The two types of ENSO. *J. Meteorol. Soc. Japan*, **71,** 273–284

Trenberth, K. E. 1975 A quasi-biennial standing wave in the southern hemisphere and interactions with sea surface temperature *Q. J. R. Meteorol. Soc.*, **101,** 55–74

Trenberth, K. E. and Shea, D. J. 1987 On the evolution of the Southern Oscillation. *Mon. Weather Rev.*, **115,** 326–332

Troup, A. J. 1965 The 'southern oscillation'. *Q. J. R. Meteorol. Soc.*, **91,** 490–506

Verma, R. K. 1994 Variability of Indian summer monsoon: relationship with global SST anomalies. *Mausam*, **45,** 205–212

Walker, G. T. 1936 'Seasonal weather and its prediction'. Pp. 117–138 in Smithsonian Report for 1935. United States Government Printing Office, Washington, USA

Walker, G. T. and Bliss, E. W. 1932 World weather V. *Mem. R. Meteorol. Soc.*, **4,** 53–84

Wallace, J. M. and Gutzler, D. S. 1981 Teleconnections in the geopotential height field during the northern hemisphere winter. *Mon. Weather. Rev.*, **109,** 784–812

Webster, P. J. and Yang, S. 1992 Monsoon and ENSO: Selectively interactive systems. *Q. J. R. Meteorol. Soc.*, **118,** 877–926

Wright, P. B. 1985 The Southern Oscillation: an ocean–atmosphere feedback system. *Bull. Am. Meteorol. Soc.*, **66,** 398–412

Xie, P. and Arkin, P. A. 1996 Analysis of global monthly precipitation using gauge observation, satellite estimates, and numerical model prediction. *J. Climate*, **9,** 840–858

Yanai, M. and Li, C.-F. 1994 'Interannual variability of the Asian summer monsoon and its relationship with ENSO, Eurasian snow cover and heating'. Pp. 27–34 in International conference on monsoon variability and prediction, Trieste, Italy. TOGA/WGNE Monsoon Numerical Experimentation Group

Yasunari, T. 1985 Zonally propagating modes of the global east–west circulation associated with the Southern Oscillation *J. Meteorol. Soc. Japan*, **63,** 1013–1029

1990 Impact of Indian monsoon on the coupled atmosphere/ocean system in the tropical Pacific. *Meteorol. Atmos. Phys.*, **44,** 29–41

1991 The monsoon year—a new concept of the climate year in the tropics. *Bull. Am. Meteorol. Soc.*, **72,** 1331–1338

Zhang, Y., Sperber, K. R. and Boyle, J. S. 1997 Climatology and interannual variation of east Asian monsoon: Results from the 1979–1995 NCEP/NCAR reanalysis. *Mon. Weather Rev.*, **125,** 2605–2619